Geochemical Perspectives Letters

Silicified seafloor contribution to TTG formation: insights from zircon O and Si isotopes

L.S. Kitoga[1,2*], M. Guitreau[1,3], J.-F. Moyen[1,4], J. Marin-Carbonne[5], M. Boyet[1], A.-S. Bouvier[5], D. Zakharov[6], G. Stevens[2]

https://doi.org/10.7185/geochemlet.2608

Abstract

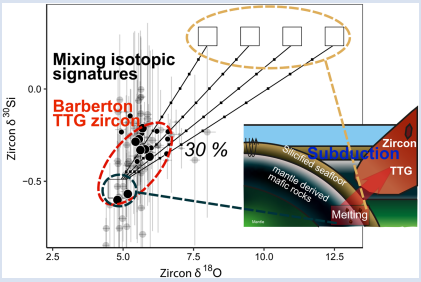

Tracing the input of altered seafloor lithologies to primary melts of tonalite-trondhjemite-granodiorite suites (TTGs) is critical for understanding Archean geodynamic processes that transported these lithologies towards melting regions. Zircon oxygen and silicon isotopic compositions in TTGs are particularly useful for this end, but their interpretation remains challenged by scarce quantitative constrains on isotopic compositions reflecting partial melting of specific Archean lithologies. Here, we combine oxygen and silicon isotope measurements in 3.45 and 3.22 Ga Barberton TTGs and their zircons with numerical models simulating partial melting of different source lithologies, which predict the isotope signatures of zircons and their host melts. Measured whole rock and zircon O and Si isotope compositions reflect the presence of up to 30 wt. % of hydrothermally silicified mafic rocks derived from the seafloor in the Barberton TTG source region. Considering the regional geological context, we propose subduction-like processes to explain the burial of the silicified seafloor into the TTG source. These results imply that subduction-like processes operated at least locally on Earth during the Paleoarchean.

Received 30 October 2025 | Accepted 4 February 2026 | Published 3 March 2026

Introduction

Geochemical signatures of buried seafloor lithologies in Archean TTGs (tonalite-trondhjemite-granodiorite) are critical for constraining seafloor alteration and burial processes on the early Earth (Trail *et al.*, 2018; André *et al.*, 2019; Deng *et al.*, 2019). TTGs are the oldest available granitic lithologies and formed by partial melting of hydrated mafic crust (Condie, 2013). Because TTG source regions likely comprised altered lithologies derived from the surface (André *et al.*, 2019; Deng *et al.*, 2019), TTGs offer a unique opportunity to investigate surface alteration processes on the early Earth. Most TTGs still contain pristine magmatic zircons, minimally affected by post-crystallisation alteration, that are texturally and compositionally distinct from zircons crystallised or modified during late stage processes (*e.g.*, metamorphism) (Guitreau *et al.*, 2022). These magmatic zircons typically serve as proxy for primary TTG melts (Trail *et al.*, 2018; Moreira *et al.*, 2020; Guitreau *et al.*, 2022; Wang *et al.*, 2022).

TTG zircon oxygen and silicon isotopic compositions are particularly powerful for tracing the reworking of Archean altered seafloor lithologies (Trail *et al.*, 2018; Wang *et al.*, 2022; Guitreau *et al.*, 2022; Lei *et al.*, 2023). This is because, compared to unaltered (mantle derived) mafic rocks exhibiting a narrow range of oxygen and silicon isotopic compositions ($\delta^{18}O_{wr} = +5.6 \pm 0.6$ ‰; Eiler *et al.*, 2000, and $\delta^{30}Si_{wr} = -0.29 \pm 0.06$‰; Savage *et al.*, 2010), altered seafloor rocks display variable oxygen and silicon isotopic compositions due to low temperature seawater-rock interactions (Abraham *et al.*, 2011; André *et al.*, 2022). Particularly, sediments and basalts that were hydrothermally silicified on the Archean seafloor (hereafter silicified seafloor lithologies) exhibit elevated $\delta^{18}O_{wr}$ (+8 to +16 ‰) and $\delta^{30}Si_{wr}$ (0 to +1.5 ‰) (Abraham *et al.*, 2011; Hofmann and Harris, 2008). If such silicified seafloor lithologies partially melted to generate felsic liquids, the latter must have inherited their unique O and Si isotopic compositions. Thus, felsic melt extraction from buried silicified seafloor lithologies to Archean TTGs can be traced by bulk rock and zircon O and Si isotope compositions in TTGs (Trail *et al.*, 2018; André *et al.*, 2019). Generally, if located within the $\delta^{18}O_{zrc}$ range of +5.3 ± 0.6 ‰ and $\delta^{30}Si_{zrc}$ range of −0.38 ± 0.04 ‰ characterising "mantle zircons" (or zircon potentially crystallised in the mantle and hosted in kimberlites; Valley *et al.*, 1998; Trail *et al.*, 2018), $\delta^{18}O_{zrc}$ and $\delta^{30}Si_{zrc}$ values of TTG hosted zircons are interpreted to evidence zircon crystallisation from felsic liquids generated by partial melting of unaltered (mantle derived) mafic rocks. Contrastingly, $\delta^{18}O_{zrc}$ and $\delta^{30}Si_{zrc}$ outside this "mantle zircon" range are generally ascribed to partial melting of altered mafic

1. Laboratoire Magmas et Volcans, Université Clermont Auvergne, CNRS-UMR6524, IRD-UMR163, OPGC, F-63000 Clermont-Ferrand, France
2. Department of Earth Sciences, University of Stellenbosch, Private Bag X1, Matieland 7602, South Africa
3. Institut Universitaire de France (IUF)
4. Département de Géologie, Université Jean Monnet, Saint-Etienne 42023, France
5. Institut des Sciences de la Terre, Université de Lausanne, 1015 Lausanne, Switzerland
6. Department of Geological and Environmental Sciences, Western Michigan University, Kalamazoo 49008, USA
* Corresponding author (email: kitogastevel@gmail.com)

lithologies or sediments, or an input of fluids from the surface (Valley *et al.*, 2005; Moreira *et al.*, 2020; Lei *et al.*, 2023). However, the mantle zircon range was originally constrained by analysing zircons from kimberlites and peridotites (Valley *et al.*, 1998; Trail *et al.*, 2018), neglecting mineral-melt O and Si isotope fractionations during partial melting and crystallisation processes (Lackey *et al.*, 2008; Guitreau *et al.*, 2022; Murphy *et al.*, 2024). Considering these fractionations can improve the determination of TTG source lithologies from bulk rock and zircon O and Si isotope analyses and the detection of altered seafloor lithology signatures in TTGs and zircons. This is important because such signatures are critical for understanding surface alteration conditions (André *et al.*, 2019) and geodynamic processes that potentially transported altered rocks towards deeper melting regions (Deng *et al.*, 2019). These processes remain debated between 1) burial below thick volcanic successions (Hernández-Uribe, 2024), 2) burial due to density driven vertical movements (Smithies *et al.*, 2021), and 3) burial due to horizontal motions linked to modern-like subduction (Deng *et al.*, 2019). Integrating isotopic data with stratigraphic and metamorphic constrains on burial depth of reworked seafloor rocks can improve the understanding of Archean geodynamic processes.

This study aims to 1) trace the signature of silicified seafloor rocks in Archean TTG source regions using zircon O and Si isotope compositions, and 2) integrate isotopic data with knowledge of regional geology to discuss geodynamic processes that transported seafloor lithologies towards melting regions. For these purposes, we present new O and Si isotope data for magmatic zircons and new O isotope data for bulk rock samples from 3.45 and 3.22 Ga TTGs occurring in the Barberton Granitoid-Greenstone Terrain (BGGT, South Africa) (Table S-1 and Fig. S-1). These new data are combined with previously published O and Si isotopic compositions of bulk rock samples and zircons from Barberton TTG (Faure and Harris, 1991; Valley *et al.*, 2005; André *et al.*, 2019; Deng *et al.*, 2019; Guitreau *et al.*, 2022; Wang *et al.*, 2022; Lei *et al.*, 2023). We also present a petrological model simulating the O and Si isotope compositions of TTG melts and zircons that reflect the reworking of unaltered mafic lithologies and silicified seafloor mafic lithologies in the TTG source region.

Results

The $\delta^{18}O_{zrc}$, $\delta^{30}Si_{zrc}$, $\delta^{18}O_{wr}$ values, major element compositions of Barberton TTG samples and images of zircons analysed in this study (Tables S-1 to S-4 and Figs. S-1 to S-3) are provided in Supplementary Information. The TTG SiO_2 content ranges between 58.2 and 73.5 wt. % and covers a large compositional spectrum from tonalite to trondhjemite (Fig. S-4), with a K_2O/Na_2O ratios of 0.22 to 0.38. Bulk $\delta^{18}O_{wr}$ values for the studied TTG samples range between +6.9 and +8.1 ‰, consistent with previously published $\delta^{18}O_{wr}$ values for Barberton TTGs (Fig. 1a) (Faure and Harris, 1991). For zircon, median $\delta^{18}O_{zrc}$ and $\delta^{30}Si_{zrc}$ values *per* analysed TTG sample range respectively from $+4.8 \pm 0.59$ to $+5.91 \pm 0.96$ ‰ and from -0.21 ± 0.34 to -0.60 ± 0.57 ‰ (Fig. 1a,b). Significant $\delta^{18}O_{zrc}$ and $\delta^{30}Si_{zrc}$ variation appear between crystals of the same sample with 2 s.d. values up to ±0.96 ‰ for $\delta^{18}O_{zrc}$ and ±0.57 ‰ for $\delta^{30}Si_{zrc}$ (Fig. 1, Tables S-1 to S-3). Important variations occur also between samples of the same pluton (*e.g.*, Nelshoogte and Stolzburg samples in Table S-1). Although samples SK-NL02 and SK-SLZ01 with the highest SiO_2 contents show the lowest zircon $\delta^{18}O_{zrc}$ and $\delta^{30}Si_{zrc}$ median values, no continuous correlation is observed between bulk rock major element features like SiO_2 content (Fig. 1a) and inter-sample or intra-pluton variations of $\delta^{18}O_{zrc}$ and $\delta^{30}Si_{zrc}$.

In the thermodynamic model (modelling methods and additional results given in SI), partial melting of an average unaltered Onverwacht basalt at 700–800 °C and 0.8–1.3 GPa along different geothermal gradients (600–900 °C/GPa) provides a liquid that is similar in major element composition to primary melts of TTGs obtained experimentally (Laurie and Stevens, 2012) and calculated empirically from compiled Barberton TTG compositions (Laurent *et al.*, 2020) (*e.g.*, K_2O/Na_2O ratio of ~0.25) (Fig. S-5). At the same P-T conditions, partial melting of the average silicified basalt produces a more potassic liquid ($K_2O/Na_2O = 3.1$ to 3.3) (Fig. S-5). Considering the proportion of residual mineral phases (Fig. S-6) and mineral/liquid fractionation coefficients (Table S-4), we modelled $\delta^{18}O$ values of +6.4 ‰ and $\delta^{30}Si$ values of −0.19 ‰ for TTG-like liquids generated by partial melting of unaltered Onverwacht basalt (or unaltered mafic source) (Fig. 2). For the liquid formed by partial melting of silicified mafic source, we obtained $\delta^{18}O_{wr}$ values of +9.5 to +14.0 ‰ (considering average $\delta^{18}O_{wr}$ variation between +10.0 and +14.5 ‰ in Onverwacht silicified rocks; Kitoga *et al.*, 2024) and $\delta^{30}Si_{wr}$ values of +0.58 to +0.56 ‰ (Fig. 2). For magmatic zircons crystallised in the melt derived from partial melting of an unaltered mafic source, we obtained $\delta^{18}O_{zrc}$ values of +4.8 to +5.0 ‰ and $\delta^{30}Si_{zrc}$ values of −0.50 to −0.60 ‰, considering zircon/liquid empirical fractionation coefficients (Lackey *et al.*, 2008; Guitreau *et al.*, 2022). Much higher $\delta^{18}O_{zrc}$ values of +8.0 to +12.5 ‰ and $\delta^{30}Si_{zrc}$ of +0.19 to +0.26 ‰ are obtained for zircons crystallised in equilibrium with the melt derived from silicified source (Fig. 2).

Discussion

Silicified seafloor lithologies in Barberton TTG source. Oxygen and silicon isotopic compositions of TTGs and their zircons are important for identifying altered seafloor lithology inputs into the TTG source regions (Trail *et al.*, 2018; André *et al.*, 2019; Deng *et al.*, 2019). Bulk rock and zircon $\delta^{18}O$ and $\delta^{30}Si$ values measured in Barberton TTGs (Fig. 1) (except in zircons from samples SK-SLZ01 and SK-NL02) are higher than isotopic values obtained in our model for felsic liquids issued by partial melting of an unaltered mantle derived mafic source and for zircon crystallised from these felsic melts (Fig. 2c). Variations of $\delta^{18}O$ and $\delta^{30}Si$ in bulk rock samples and zircons do not show a continuous correlation with bulk rock SiO_2 concentrations (Fig. 1). Such a continuous correlation typically reflects isotopic variation due to magmatic differentiation of a primary melt and/or crust assimilation (Lackey *et al.*, 2008; Savage *et al.*, 2011; Guitreau *et al.*, 2022). The lack of continuous correlation between isotopic compositions and SiO_2 in Barberton TTGs (Fig. 1) precludes an important control of magmatic differentiation on measured isotopic compositions.

In $\delta^{18}O$ *versus* $\delta^{30}Si$ diagram (Fig. 3), Barberton TTGs and their zircons plot on mixing curves between end member isotopic signatures reflecting partial melting of an unaltered mafic source and a silicified seafloor source. Mixing unaltered mafic lithologies with up to ~30 % of silicified seafloor rocks in the melting region accounts for the measured isotopic compositions, consistent with estimates of André *et al.* (2019). We note, however, that the lowest $\delta^{18}O_{zrc}$ and $\delta^{30}Si_{zrc}$ values observed in samples SK-SLZ01 and SK-NL02 mimic the modelled zircon end member composition reflecting partial melting of an unaltered mafic lithology (Fig. 3). These particular zircons (and others displaying similar $\delta^{18}O_{zrc}$ values in the literature, *e.g.*, Moreira *et al.*, 2020; Smithies *et al.*, 2021) likely reflect a so far undocumented end member for Archean magmatic zircons crystallised in felsic liquids generated mainly by partial melting of an unaltered mafic lithology. This interpretation is also consistent with sample

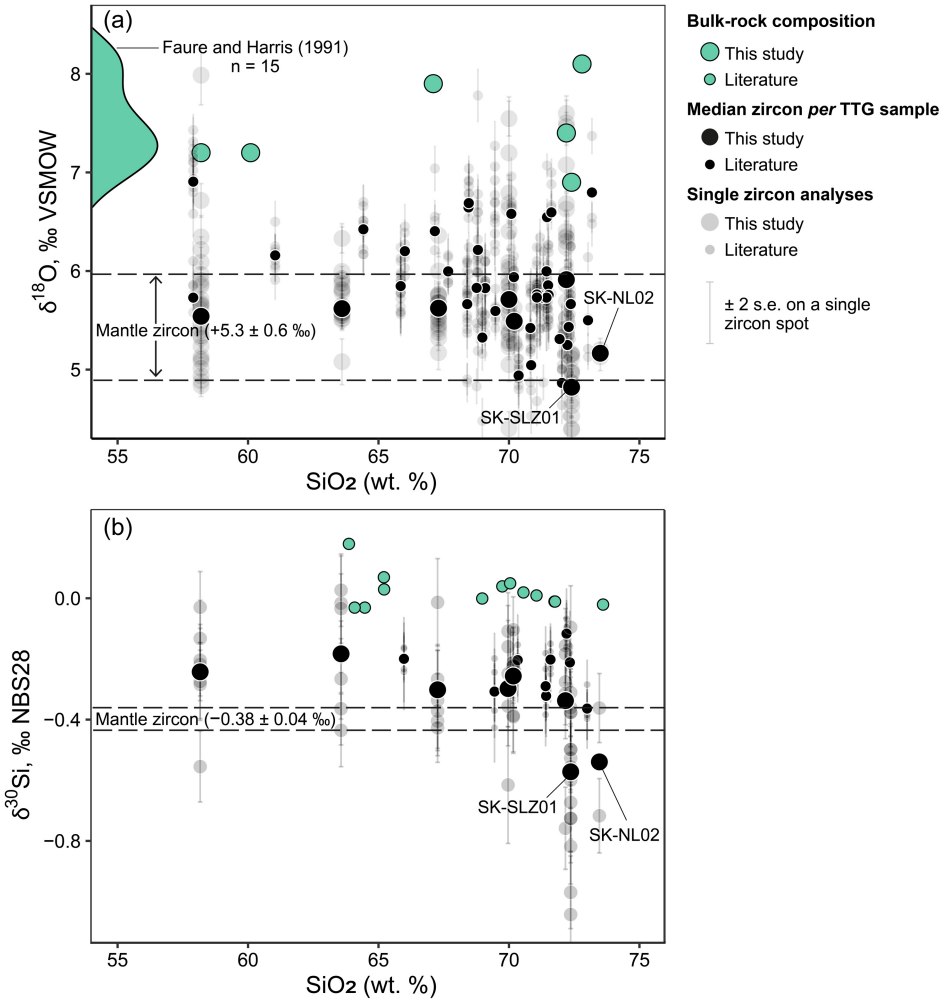

Figure 1 Oxygen and silicon isotopic composition of bulk rock and zircon samples from the BGGT plotted against bulk rock SiO_2 concentration. Error bars are 2 s.e. uncertainty for every spot. Density curve in **(a)** presents $\delta^{18}O_{wr}$ values in 15 samples from the Kaap Valley pluton (BGGT) from Faure and Harris (1991). Other Barberton TTG data sources: $\delta^{18}O_{zrc}$ in **(a)** (Valley *et al.*, 2005; Wang *et al.*, 2022; Lei *et al.*, 2023), and whole rock $\delta^{30}Si_{wr}$ in **(b)** (André *et al.*, 2019; Deng *et al.*, 2019), $\delta^{30}Si_{zrc}$ (Guitreau *et al.*, 2022; Lei *et al.*, 2023). The 'mantle zircon' range represents $\delta^{18}O_{zrc}$ and $\delta^{30}Si_{zrc}$ values of zircons from peridotites and kimberlites (Trail *et al.*, 2018).

SK-SLZ01 showing the lowest whole rock $\delta^{18}O_{wr}$ of our dataset, although bulk rock compositions generally do not preserve this end member signature in Barberton TTGs.

Recently, a controversy on Barberton TTG source lithologies arose from interpretations of $\delta^{18}O$ and $\delta^{30}Si$ values of their bulk rock samples and zircons. Wang *et al.* (2022) interpreted 3.45 Ga Barberton TTG zircons with $\delta^{18}O_{zrc}$ signatures within the range of mantle zircons as demonstrating the absence of silicified seafloor rocks in the TTG source region. Conversely, $\delta^{30}Si_{zrc}$ (Guitreau *et al.*, 2022; Lei *et al.*, 2023) and $\delta^{30}Si_{wr}$ values (André *et al.*, 2019; Deng *et al.*, 2019) within the same Barberton TTGs were ascribed to the presence of silicified seafloor lithologies in the source regions. These contradictory interpretations result from considering that zircons with $\delta^{18}O_{zrc}$ of +5.3 ± 0.6 ‰ and $\delta^{30}Si_{zrc}$ of −0.38 ± 0.04 ‰ (mantle zircon ranges; Fig. 1b), necessarily crystallised from melts formed by partial melting of unaltered mafic lithologies. Our model reveals that zircons reflecting an unaltered mantle derived source for TTGs are restricted to a $\delta^{18}O_{zrc}$ of +4.8 to +5.0 ‰ and $\delta^{30}Si_{zrc}$ of −0.5 to −0.6‰ (Fig. 2). When modelled end member compositions are mixed, $\delta^{18}O_{zrc}$ and $\delta^{30}Si_{zrc}$ appear to be well coupled in Barberton TTGs and reflect a contribution of silicified seafloor lithologies to the TTG melt (Fig. 3). Our dataset shows no $\delta^{18}O_{zrc}$ variation over time, although Wang *et al.* (2022) observed an increase of $\delta^{18}O_{zrc}$ at ~3.23 Ga in Barberton TTGs. The highest $\delta^{18}O_{zrc}$ (exceeding 5.9 ‰) were measured only in post-3.23 Ga Honingklip, Eerstehoek and Uitgevonden bodies (Fig. S-1) by Wang *et al.* (2022) (not analysed here), and may reflect incorporation of silicified seafloor lithologies with a higher $\delta^{18}O$ value, by the source region of these specific plutons (Kitoga *et al.*, 2024). Unlike that proposed by Wang *et al.* (2022), these high $\delta^{18}O_{zrc}$ values do not date the onset of seafloor recycling at ~3.23 Ga because seafloor derived rocks were also present in the source region of ~3.45 Ga old Stolzburg and Theespruit TTGs as well as 3.28–3.23 Ga old Kaap Valley and Nelshoogte TTGs investigated here (Fig. 3).

More importantly, our results demonstrate that Paleoarchean TTG zircons with $\delta^{18}O_{zrc}$ or $\delta^{30}Si_{zrc}$ values within the range of mantle zircon do not necessarily reflect an unaltered mafic source for TTG melts. Interestingly, the $\delta^{18}O_{zrc}$ and $\delta^{30}Si_{zrc}$ values previously published for ≥ 3.0 Ga TTG hosted and detrital zircons in the Pilbara Craton, Saglek, North China Craton and Coorg block (Fig. 3; references listed in Table S-5) are also generally higher than signatures reflecting the partial melting of an unaltered mafic source. Consequently, partial melting of silicified seafloor rocks potentially contributed to Paleoarchean TTG melts worldwide.

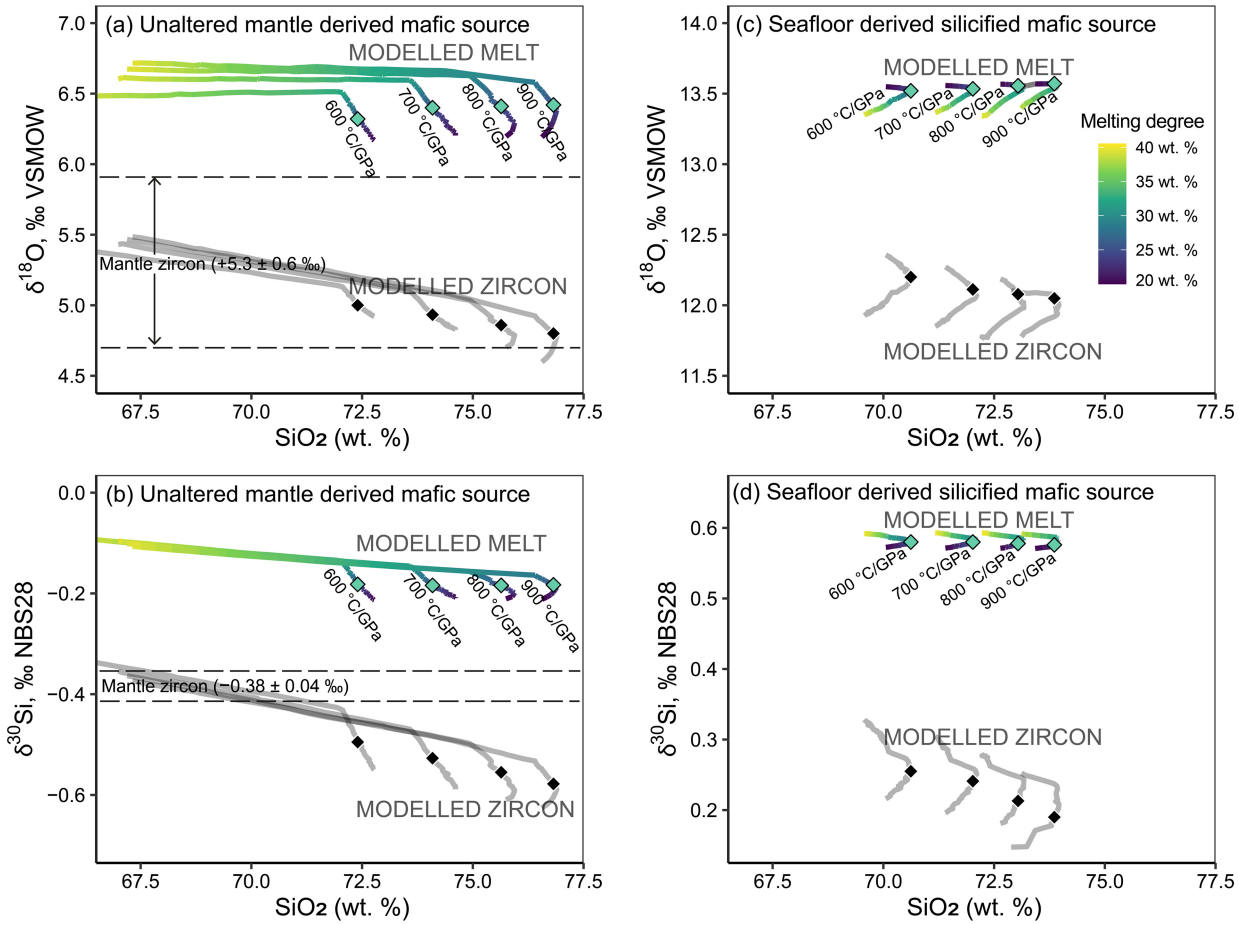

Figure 2 Modelled melt and zircon isotopic compositions reflecting partial melting of an unaltered mafic source and a silicified source along different P-T paths. We considered melting degrees between 20 and 40 wt. % (able to produce TTG-like melts) (Laurie and Stevens, 2012). Plotted SiO_2 concentrations are calculated on an anhydrous basis. Diamonds represent conditions where partial melting of a basaltic source generates a melt with TTG-like major element composition. In **(c)** we only considered an average $\delta^{18}O_{wr}$ of +13.5 ‰ for a silicified mafic source (overlooking the full $\delta^{18}O_{wr}$ variation shown in Fig. 3 for simplicity).

Evidence of Paleoarchean subduction-like processes in the Barberton area. The presence of silicified rocks in TTG source regions complements evidence from Nd-Hf isotopes that the mafic source of Barberton TTGs was extracted from the mantle less than 0.3 Ga before being reworked (Moyen *et al.*, 2019). These observations collectively support 3.5–3.2 Ga old rocks of the Onverwacht Group as proxies of lithologies melted to form 3.45 and 3.22 Ga Barberton TTGs (André *et al.*, 2022; Kitoga *et al.*, 2024). Thus, to constrain geodynamic processes that may have buried silicified seafloor lithologies into melting regions, we interpret our isotopic constrains in light of geological information on the stratigraphic burial and regional metamorphism of Onverwacht silicified rocks before episodes of TTG magmatism (Hofmann and Harris, 2008; Byerly *et al.*, 2019).

Within the BGGT and surrounding Paleoarchean terranes (Byerly *et al.*, 2019), there is no evidence (*e.g.*, particularly thick stratigraphic layers) of an important volcanic and/or sedimentary event capable of burying the silicified rocks to the depth (>20km) required for their partial melting ~3.45 and ~3.2 Ga ago, as would be needed in a stagnant crust scenario (Moyen *et al.*, 2019). This precludes partial melting of altered basalts at the base of an over-thickened volcano-sedimentary succession (Hernández-Uribe, 2024) as a viable explanation for the formation of BGGT TTGs. At the time of TTG magmatism in the BGGT, the silicified seafloor lithologies of the Onverwacht Group were not stratigraphically buried deeper than 10 km below the surface by younger volcanic or sedimentary piles. Thus, vertical movements of delamination or dripping (Van Kranendonk *et al.*, 2014) are also unlikely to explain their transport towards TTG source regions as these vertical movements should preferentially mobilise lower crustal material. In addition, if overturn movements proposed by Schmitz and Heubeck (2021) controlled the recycling of silicified rocks into the TTG source region, at 3.48 to 3.20 Ga, a 10 km thick volcano-sedimentary succession would not be as continuously preserved with greenschist metamorphic facies, as it actually is in Barberton (Byerly *et al.*, 2019).

Discarding alternatives favours subduction-like processes (Stevens *et al.*, 2002; Moyen *et al.*, 2006) to explain the reworking of seafloor silicified rocks in the Barberton TTG source regions. A horizontally mobile portion of the Paleoarchean crust was likely subducted below a relatively stagnant (and therefore more easily preserved) portion of the same crust due to vigorous mantle convection. This model accounts for both geochemical evidence of reworked silicified seafloor, preservation of a ~10 km thick, continuous volcano-sedimentary succession that has never exceeded greenschist facies in northern BGGT, and rapid subduction of sediments proposed around 3.2 Ga ago by petrochronological analyses in southern BGGT (Stevens *et al.*, 2002; Moyen *et al.*, 2006). It is, however, important to note that this proposed localised subduction does not necessarily imply global subduction worldwide in the Paleoarchean. In fact, in other Paleoarchean terrains such as the Pilbara craton, density driven

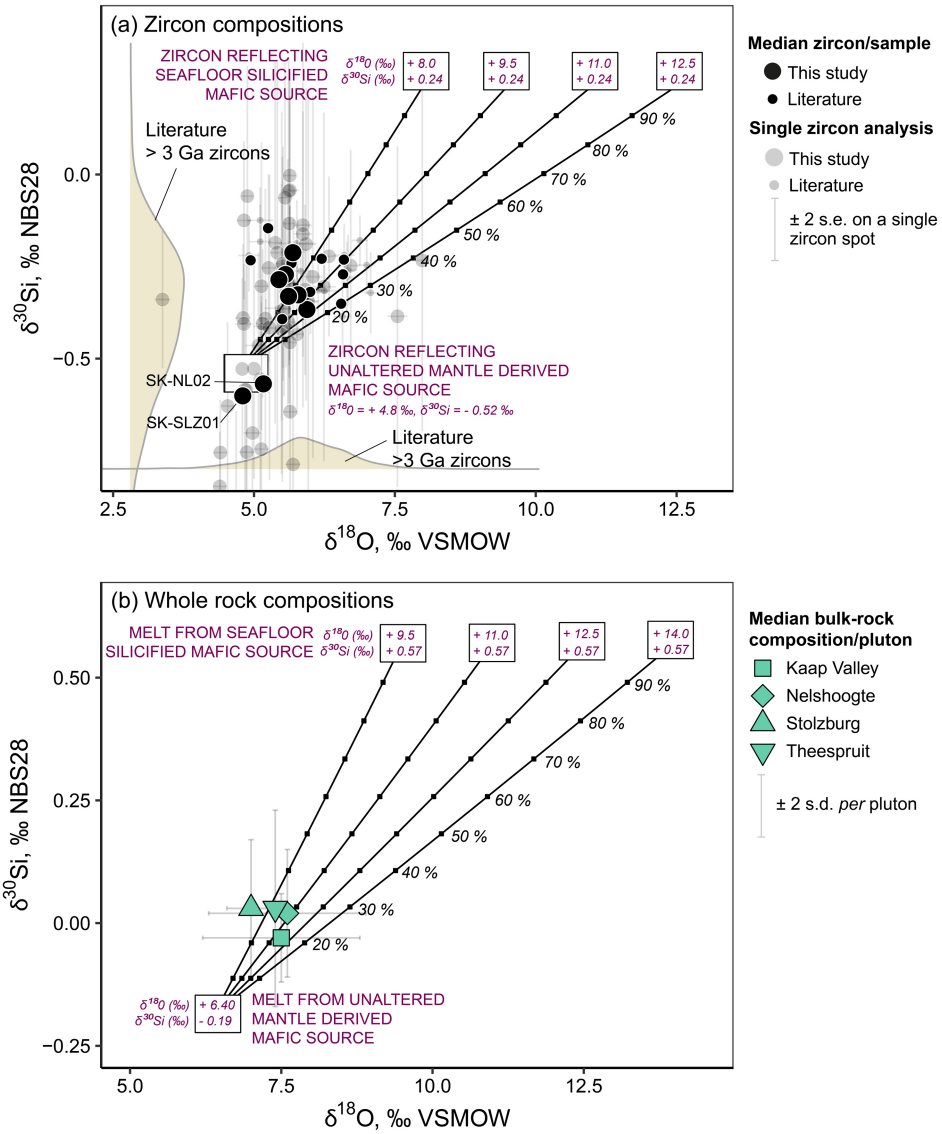

Figure 3 Mixing model explaining the origin of oxygen and silicon isotopic compositions of **(a)** BGGT TTG zircon and **(b)** whole rock samples. Density curves in **(a)** are distributions of $\delta^{18}O_{zrc}$ and $\delta^{30}Si_{zrc}$ in other Paleoarchean or older zircons (references in Table S-5). The two end member source signatures considered in the mixing calculations result from our numerical model. Zircon compositions on mixing curves represent the calculated isotopic composition of zircon crystallised from modelled liquids (end member or mixed). Average $\delta^{18}O_{wr}$ temporal variation in Onverwacht silicified lavas (Kitoga *et al.*, 2024) is considered.

vertical transportation was proposed as the most likely geodynamic scenario by both geological and isotopic data (Smithies *et al.*, 2019). Co-occurrence of different reworking processes on the Paleoarchean Earth remains a possibility.

Acknowledgement

The study benefited from financial support of CNRS, the South-African NRF under the international BUCOMO project, and French Agence Nationale de la Recherche (ANR-10-LABX-0006). Doctoral funding was also awarded to LSK by CNRS. We thank M.V. Leandro for companionship in the field, Clara Gorce, Syro Lacerda and Thomas Bovay for help during sample preparation, Emmy Voyer for technical expertise during CL imaging and Mareli Grobbelaar for assistance with major element analyses. Benita Putlitz and Torsten Vennemann are thanked for facilitating whole rock oxygen isotope measurements. We also sincerely thank Jean-Baptiste Combaz, Oscar Laurent, Emilie Bruand and Prof. Luc André for insightful discussions during the preparation of this manuscript. We thank the editor, Romain Tartèse, and the two anonymous reviewers for their comments and recommendations that allowed improving this manuscript. This is contribution no. 743 of the ClerVolc program of the International Research Center for Disaster Sciences and Sustainable Development of the University of Clermont Auvergne.

Editor: Romain Tartèse

Additional Information

Supplementary Information accompanies this letter at https://www.geochemicalperspectivesletters.org/article2608.

Cite this letter as: Kitoga, L.S., Guitreau, M., Moyen, J.-F., Marin-Carbonne, J., Boyet, M., Bouvier, A.-S., Zakharov, D., Stevens, G. (2026) Silicified seafloor contribution to TTG formation: insights from zircon O and Si isotopes. *Geochem. Persp. Let.* 39, 22–27. https://doi.org/10.7185/geochemlet.2608

References

Abraham, K., Hofmann, A., Foley, S.F., Cardinal, D., Harris, C., Barth, M.G., Andre, L. (2011) Coupled silicon-oxygen isotope fractionation traces Archaean silicification. *Earth and Planetary Science Letters 301,* 222–230. https://doi.org/10.1016/j.epsl.2010.11.002

André, L., Abraham, K., Hofmann, A., Monin, L., Kleinhanns, I.C., Foley, S. (2019) Early continental crust generated by reworking of basalts variably silicified by seawater. *Nature Geoscience*. https://doi.org/10.1038/s41561-019-0408-5

André, L., Monin, L., Hofmann, A. (2022) The origin of early continental crust: New clues from coupling Ge/Si ratios with silicon isotopes. *Earth and Planetary Science Letters 582*. https://doi.org/10.1016/j.epsl.2022.117415

Byerly, G.R., Lowe, D.R., Heubeck, C. (2019) Geologic Evolution of the Barberton Greenstone Belt—A Unique Record of Crustal Development, Surface Processes, and Early Life 3.55–3.20 Ga. *Earth's Oldest Rocks*, Elsevier, 569–613. https://doi.org/10.1016/b978-0-444-63901-1.00024-1

Condie, K.C. (2013) How to Make a Continent: Thirty-five Years of TTG Research. In: Dilek, Y., Furnes, H. (Eds.) *Evolution of Archean crust and early life*. Springer, 179–193. https://doi.org/10.1007/978-94-007-7615-9

Deng, Z., Chaussidon, M., Guitreau, M., Puchtel, I.S., Dauphas, N. (2019) An oceanic subduction origin for Archean granitoids revealed by silicon isotopes. *Nature Geoscience 12,* 774–779. https://doi.org/10.1038/s41561-019-0407-6

Eiler, J.M., Crawford, A., Elliott, T., Farley, K.A., Valley, J.W., Stolper, E.M. (2000) Oxygen isotope geochemistry of oceanic-arc lavas. *Journal of Petrology 41,* 229–256. https://doi.org/10.1093/petrology/41.2.229

Faure, K., Harris, C. (1991) Oxygen and carbon isotope geochemistry of the 3. 2 Ga Kaap Valley tonalite, Barberton greenstone belt, South Africa. *Precambrian Research* 52, 301–319.

Guitreau, M., Gannoun, A., Deng, Z., Chaussidon, M., Moynier, F., Barbarin, B., Marin-Carbonne, J. (2022) Stable isotope geochemistry of silicon in granitoid zircon. *Geochimica et Cosmochimica Acta 316,* 273–294. https://doi.org/10.1016/j.gca.2021.09.029

Hernández-Uribe, D. (2024) Generation of Archaean oxidizing and wet magmas from mafic crustal overthickening. *Nature Geoscience* 8–10. https://doi.org/10.1038/s41561-024-01489-z

Hofmann, A., Harris, C. (2008) Silica alteration zones in the Barberton greenstone belt: A window into subseafloor processes 3.5-3.3 Ga ago. *Chemical Geology* 257, 224–242. https://doi.org/10.1016/j.chemgeo.2008.09.015

Kitoga, L.S., Zakharov, D., Marin-Carbonne, J., Boyet, M., Moyen, J.-F., Di Rocco, T., Pack, A., Olivier, N., Stevens, G. (2024) Oxygen and silicon isotopic compositions of Archean silicified lava and cherts of the Onverwacht Group: Implication for seafloor hydrothermalism and the nature of recycled components in the source of granitoids. *Chemical Geology,* 122407. https://doi.org/10.1016/j.chemgeo.2024.122407

Lackey, J.S., Valley, J.W., Chen, J.H., Stockli, D.F. (2008) Dynamic magma systems, crustal recycling, and alteration in the Central Sierra Nevada batholith: The oxygen isotope record. *Journal of Petrology 49,* 1397–1426. https://doi.org/10.1093/petrology/egn030

Laurent, O., Björnsen, J., Wotzlaw, J.-F., Bretscher, S., Pimenta Silva, M., Moyen, J.-F., Ulmer, P., Bachmann, O. (2020) Earth's earliest granitoids are crystal-rich magma reservoirs tapped by silicic eruptions. *Nature Geoscience 13,* 163–169. https://doi.org/10.1038/s41561-019-0520-6

Laurie, A., Stevens, G. (2012) Water-present eclogite melting to produce Earth's early felsic crust. *Chemical Geology* 314–317, 83–95. https://doi.org/10.1016/j.chemgeo.2012.05.001

Lei, K., Wang, H., Wang, X., Zhang, Q., Li, X. (2023) Decoupled Zircon Si–O Isotopes Tracing the Supracrustal Silicification and Komatiitic-Derived Fluids in the Source of TTGs. *Geophysical Research Letters 50,* 1–9. https://doi.org/10.1029/2023GL104002

Moreira, H., Storey, C., Fowler, M., Seixas, L., Dunlop, J. (2020) Petrogenetic processes at the tipping point of plate tectonics: Hf-O isotope ternary modelling of Earth's last TTG to sanukitoid transition. *Earth and Planetary Science Letters 551.* https://doi.org/10.1016/j.epsl.2020.116558

Moyen, J.-F., Stevens, G., Kisters, A.F.M., Belcher, R.W., Lemirre, B. (2019) TTG Plutons of the Barberton Granitoid-Greenstone Terrain, South Africa. *Earth's Oldest Rocks,* Elsevier, 607–667. https://doi.org/10.1016/b978-0-444-63901-1.00025-3

Moyen, J.F., Stevens, G., Kisters, A. (2006) Record of mid-Archaean subduction from metamorphism in the Barberton terrain, South Africa. *Nature 442,* 559–562. https://doi.org/10.1038/nature04972

Murphy, M.E., Macdonald, J.E., Fischer, S., Gardiner, N.J., White, R.W., Savage, P.S. (2024) Silicon isotopes in an Archaean migmatite confirm seawater silicification of TTG sources. *Geochimica et Cosmochimica Acta 368,* 34–49. https://doi.org/10.1016/j.gca.2024.01.018

Savage, P.S., Georg, R.B., Armytage, R.M.G., Williams, H.M., Halliday, A.N. (2010) Silicon isotope homogeneity in the mantle. *Earth and Planetary Science Letters 295,* 139–146. https://doi.org/10.1016/j.epsl.2010.03.035

Savage, P.S., Georg, R.B., Williams, H.M., Burton, K.W., Halliday, A.N. (2011) Silicon isotope fractionation during magmatic differentiation. *Geochimica et Cosmochimica Acta 75,* 6124–6139. https://doi.org/10.1016/j.gca.2011.07.043

Schmitz, M., Heubeck, C. (2021) Constraints on deformation mechanisms of the Barberton Greenstone Belt from regional stratigraphic and structural data of the synorogenic Moodies Group. *Precambrian Research 362,* 106177. https://doi.org/10.1016/j.precamres.2021.106177

Smithies, R.H., Lu, Y., Johnson, T.E., Kirkland, C.L., Cassidy, K.F., Champion, D.C., Mole, D.R., Zibra, I., Gessner, K., Sapkota, J., De Paoli, M.C., Poujol, M. (2019) No evidence for high-pressure melting of Earth's crust in the Archean. *Nature Communications 10.* https://doi.org/10.1038/s41467-019-13547-x

Smithies, R.H., Lu, Y., Kirkland, C.L., Johnson, T.E., Mole, D.R., Champion, D.C., Martin, L., Jeon, H., Wingate, M.T.D., Johnson, S.P. (2021) Oxygen isotopes trace the origins of Earth's earliest continental crust. *Nature 592.* https://doi.org/10.1038/s41586-021-03337-1

Stevens, G., Droop, G.T.R., Armstrong, R.A., Anhaeusser, C.R. (2002) Amphibolite facies metamorphism in the Schapenburg schist belt: A record of the mid-crustal response to ~3.23 Ga terrane accretion in the Barberton greenston belt.pdf. *South African Journal of Geology* 105, 271–284.

Trail, D., Boehnke, P., Savage, P.S., Liu, M.C., Miller, M.L., Bindeman, I. (2018) Origin and significance of Si and O isotope heterogeneities in Phanerozoic, Archean, and Hadean zircon. *Proceedings of the National Academy of Sciences of the United States of America* 115, 10287–10292. https://doi.org/10.1073/pnas.1808335115

Valley, J.W., Kinny, P.D., Schulze, D.J., Spicuzza, M.J. (1998) Zircon megacrysts from kimberlite: Oxygen isotope variability among mantle melts. *Contributions to Mineralogy and Petrology 133,* 1–11. https://doi.org/10.1007/s004100050432

Valley, J.W., Lackey, J.S., Cavosie, A.J., Clechenko, C.C., Spicuzza, M.J., Basei, M.A.S., Bindeman, I.N., Ferreira, V.P., Sial, A.N., King, E.M., Peck, W.H., Sinha, A.K., Wei, C.S. (2005) 4.4 billion years of crustal maturation: Oxygen isotope ratios of magmatic zircon. *Contributions to Mineralogy and Petrology* 150, 561–580. https://doi.org/10.1007/s00410-005-0025-8

Van Kranendonk, M.J., Kröner, A., Hoffman, J.E., Nagel, T., Anhaeusser, C.R. (2014) Just another drip: Re-analysis of a proposed mesoarchean suture from the Barberton mountain land, South Africa. *Precambrian Research 254,* 19–35. https://doi.org/10.1016/j.precamres.2014.07.022

Wang, X., Tang, M., Moyen, J., Wang, D., Kröner, A., Xia, X., Xie, H., Anhaeusser, C., Hofmann, A., Li, J., Li, L. (2022) The onset of deep recycling of supracrustal materials at the Paleo-Mesoarchean boundary. *National Science Review 9,* 1–9. https://doi.org/10.1093/nsr/nwab136

Geochemical Perspectives Letters

Silicified seafloor contribution to TTG formation: insights from zircon O and Si isotopes

L.S. Kitoga, M. Guitreau, J-F. Moyen, J. Marin-Carbonne, M. Boyet, A-S. Bouvier, D. Zakharov, G. Stevens

Supplementary Information

The Supplementary Information includes:

- Geological setting and samples
- Analytical methods (Sample preparation, Cathodoluminescence imaging, SIMS analysis of zircon oxygen isotope compositions, LA-ICP-MS measurements of zircon silicon isotope compositions, laser-fluorination analysis of bulk-rock O isotope composition, XRF analysis of bulk-rock major element composition)
- Numerical modelling (Thermodynamic phase equilibrium modelling, modelling melt's O and Si isotope composition, Calculation of the O and Si isotopic composition of theoretical magmatic zircons)
- Tables S-1 to S-5
- Figures S-1 to S-6
- Supplementary Information References

Geological setting and samples

The Barberton Granitoid-Greenstone Terrain (BGGT) in South Africa exposes a succession of supracrustal rocks known as the Barberton Greenstone Belt (BGB) and a series of surrounding granitoids (Byerly *et al.*, 2019; Lowe and Byerly, 2007; Moyen *et al.*, 2019) (**Fig. S-1**). The supracrustal successions constituting the BGB are subdivided into three different groups, namely the 3.53-3.30 Ga Onverwacht Group, 3.28-3.25 Ga Fig Tree Group and ~3.2 Ga Moodies Group. The oldest Onverwacht Group of the BGB comprises meta-volcanic rocks (generally ultramafic to mafic but occasionally felsic) that are generally overlain by sedimentary layers encompassing pyroclastites, detritic and orthochemical metasediments. The sedimentary layers and the top of lava flows are generally silicified in the Onverwacht Group due to low-temperature hydrothermalism near the Paleoarchean seafloor (Hofmann and Harris, 2008).

The BGB is surrounded by four different generations of Paleoarchean to Mesoarchean granitoids (Moyen *et al.*, 2019; Moyen *et al.*, 2021). The first generation of granitoids is represented by the 3.51 Ga Steynsdorp tonalite-trondhjemite-granodiorite (TTG) pluton which crops out in the southwestern part of the BGGT. The second generation emplaced at ~3.45 Ga includes the Theespruit and Stolzburg TTG plutons that crop out in the south of the BGGT. The third granitoid

generation is represented by 3.28-3.22 Ga TTG bodies which include the Kaap Valley and Nelshoogte plutons both appearing in the east of the BGGT. Finally, the last granitoid generation of the BGGT is represented by large ~3.1 Ga granodiorite-monzonite-syenogranite (GMS) plutons which comprise the Boesmanskop, Heerenveen, Mpuluzi, Pig's Peak and Nelspruit intrusions.

For the present study, we have collected and analysed eleven samples of the Barberton TTGs (**Fig. S-1**). The samples originated from the ~3.45 Ga Stolzburg pluton (n=2, SK-SLZ01 and SK-SLZ02), the ~3.45 Ga Theespruit pluton (n=1, SK-THP03), the 3.22 Ga Nelshoogte pluton (n=4, SK-NL01, SK-NL02, SK-NL03 and SK-NL04) and the ~3.22 Ga Kaap Valley pluton (n=4, SK-KV01, SK-KV02, SK-KV03 and SK-KV04). Our samples, therefore, represent two different generations of Paleoarchean felsic magmatic events in the BGGT (i.e. the ~3.45 and the 3.22 Ga events). In addition, our sample set is also representative of the lithological heterogeneity of the Barberton TTG plutons which range from tonalitic to trondhjemitic compositions (**Table S-1** and **Fig. S-2**).

Analytical methods

Sample preparation

Centimetre-thick slabs of individual hand-specimen samples were cut using a diamond saw and used for powder preparation at Stellenbosch University and zircon separation at Laboratoire Magmas et Volcans (Clermont Auvergne University). A tungsten carbide jaw crusher and an agate mill were successively used to prepare the fine rock powders. For zircon separation, selected rock slabs were firstly crushed and sieved to separate minerals of different sizes. Subsequently, a Frantz magnetic separator was used to eliminate magnetic minerals, and was followed by flotation in a dense liquid (bromoform, density = 2.89) to isolate the fraction of dense minerals, including zircon. Zircon was finally hand-picked under a binocular microscope and mounted in epoxy, which was then polished to flatness and carefully cut using a diamond wire saw into smaller portions carrying relevant zircons. These portions of the epoxy mount were pressed into an indium mount along with polished specimens of 91500 zircon standard at the University of Lausanne. The replacement of as much epoxy as possible by indium before analyses was important for minimising signal perturbations due to epoxy degassing during secondary ion mass spectrometry analyses. Interferometric analyses of the prepared indium mount demonstrated that the elevation gradient at its surface did not exceed 5 micrometres.

Cathodoluminescence imaging

Cathodoluminescence (CL) images of the mounted zircons were acquired at Laboratoire Magmas et Volcans using Jeol JSM-5910LV scanning electron microscope to select the most preserved areas of the mounted zircons for isotopic analyses. These images were acquired at an accelerating voltage of 15 kV. The CL images of analysed zircon areas typically featured oscillatory or sector zoning that are characteristic of igneous zircons (**Fig. S-2**). We purposely avoided, as much as possible, cracks, patchy domains, weathered/altered domains and visible metamorphic overgrowths/recrystallized zones so as to retrieve the most pristine isotopic signal for meaningful interpretations.

SIMS analysis of zircon oxygen isotope compositions

The oxygen isotope compositions of zircons grains separated from eight different samples were measured at the University of Lausanne by secondary ion mass spectrometry (SIMS) using the 1280 Swiss-SIMS instrument. Depending on the number of separated zircons, 1 to 15 zircon grains per sample and up to two spots per grain were analysed. The analyses were conducted with a ~15 µm spot using a 10 kv Cs^+ primary beam and a 2 nA current. After introduction into the spectrometer through a slit of ~122 micrometres, the $^{16}O^-$ and $^{18}O^-$ secondary ion beams passed through an exit slit 1 towards the respective off-axis L'2 (with a 10^{10} ohm resister) and H1 Faraday cups (with a 10^{11} ohm resister) in

multi-collection mode. This analytical setting resulted in a mass resolving power of ~2400 on ^{18}O detector. Individual analyses lasted 3.5 minutes including the duration of pre-analysis sputtering, automatic centering of the secondary ion beams and 20 cycles of counting, each of which lasted 5 seconds. Oxygen isotope compositions are expressed in delta notation representing a permil deviation of the analysed $^{18}O/^{16}O$ ratio from that of VSMOW ($\delta^{18}O=1000*(^{18}O/^{16}O)_{sample}/(^{18}O/^{16}OV)_{SMOW}-1000$). Repeated analyses of 91500 zircon standard ($\delta^{18}O$ = +9.9 ± 0.3 ‰) (Wiedenbeck *et al.*, 2004) mounted in the same indium mount as our zircon crystals were used to control the stability of the signal over the analytical session, to correct for instrumental mass fractionation, and to evaluate the reproducibility of the analyses. The 91500 zircon standard measurements allowed estimating an external reproducibility of 0.4 ‰ (2 SD; n=29) (**Table S-2**).

LA-MC-ICP-MS measurements of zircon silicon isotope compositions

The silicon isotope composition of zircons was analysed at Laboratoire Magmas et Volcans by laser-ablation multi-collection inductively coupled plasma mass spectrometry (LA-MC-ICP-MS), using a Resonetics Resolution M-50E and a Thermo Scientific Neptune Plus MC-ICP-MS. Up to 7 zircon grains per sample and 2 spots per grain were measured for Si isotope compositions. These measurements followed the procedure previously published by Guitreau *et al.* (2020). Briefly, an excimer laser characterised by a wavelength of 193 nm and an energy of 2-5 mJ was used to ablate zircon crystals with a 40 µm spots. The generated particles were carried into the mass spectrometer through a He gas flow at a rate of ~0.65 L/min. Counting operated in static multi-collection mode and the external L3 and H3 Faraday cups served for counting ^{28}Si and ^{30}Si ions respectively, whereas the ^{29}Si ions were counted on the central C cup. Individual analyses comprised 20 seconds of background measurement followed by ~70 seconds of analyses during which 70 different counting cycles were performed. Silicon isotope compositions are expressed in delta notation representing a permil deviation of the analysed $^{30}Si/^{28}Si$ ratio from that of NBS28 standards ($\delta^{30}Si=1000*(^{30}Si/^{28}Si)_{sample}/(^{30}Si/^{28}Si)_{NBS28}-1000$). Measurements of unknowns were bracketed by analyses of 91500 zircon standard that was used as an external reference for standard bracketing. Repeated analyses of Mud-Tank ($\delta^{30}Si$ = -0.36 ± 0.34 ‰, 2 SD, n=12) and MUN-4 ($\delta^{30}Si$ = -1.84 ± 0.33 ‰, 2 SD, n=12) used as secondary zircon standards gave results consistent with those of the literature (Mud-Tank $\delta^{30}Si$ = -0.34 ± 0.03 ‰, Trail *et al.*, 2018; MUN-4 $\delta^{30}Si$ = -2.05 ± 0.30 ‰, Guitreau *et al.*, 2020) (**Table S-3**).

Laser-fluorination analysis of bulk-rock O isotope composition

The bulk-rock O isotope compositions of 2 tonalitic and 4 trondhjemitic samples were measured at the University of Lausanne by laser-fluorination mass spectrometry using a MAT253 instrument. These data were analysed jointly with the bulk-quartz O isotope composition reported in Kitoga *et al.* (2024), with an external reproducibility of 0.2 ‰ (2 SD) estimated based on repeated analyses of LS1 quartz standard ($\delta^{18}O$ = 18.1 ‰) throughout the analytical session.

XRF analysis of bulk-rock major element composition

Major element compositions were analysed at Stellenbosch University using a PAN analytical Axios Wavelength Dispersive x-ray fluorescence (XRF) spectrometer. Homogeneous discs, representative of each sample, on which these measurements were performed, had been prepared by mixing 0.5 g of powder with 5 g of flux (32.8 % $LiBO_2$ + 66.7 % $Li_2B_4O_7$ + 0.5 % LiI) and fusing the mixture at 1000 ° C in an automatic Claisse M4 Gas Fusion instrument. Several reference materials (BE-N, JB-1, BHVO-A, JG-1, HUSG-1 and WITS-G) were analysed repetitively along with the samples and returned an external reproducibility (2 SD) that was lower than 0.7 wt. % for SiO_2 and Al_2O_3, and 0.1 wt. % for all the other major oxides (see here https://commons.datacite.org/doi.org/10.25519/qxr1-9y88 the dataset including reference material analyses). The reference materials further allowed estimating an accuracy of ± 5 % (2 SD) for the

reported major element compositions. The volatile content or loss on ignition (LOI) was measured gravimetrically after keeping small portions of rock powders in a muffle furnace at 1000° C for a duration of 30 minutes.

Numerical modelling

To explain the origin of Si and O isotopic compositions measured in bulk TTG and zircon samples, we have simulated the composition of felsic melts formed by partial melting of an average unaltered basalt and an average silicified basalt. We further calculated the Si and O isotope composition of zircons that would crystallise from these felsic melts. Three different tasks were achieved during this numerical simulation:

- Thermodynamic determination of the nature and proportion of mineral phases as well as the proportion and composition of the melt existing at different P-T conditions (results shown in **Fig. S-5** and **Fig. S-6**)
- Calculation of the O and Si isotopic compositions of the generated melt (based on liquid/solid partitioning of O and Si isotopes);
- Estimation of the O and Si isotopic composition of zircons precipitated from the melt based on melt/zircon partitioning of O and Si isotopes.

Thermodynamic phase equilibrium modelling

We used the Perple_X software incorporating the thermodynamic database and solution models of Holland *et al.* (2018) and Holland & Powell (2011) to model the evolution of an average silicified or an average unaltered mafic source in closed system within the temperature and pressure ranges of 550 to 1020 °C and 0.5 to 1.7 GPa. Ten different oxides were considered in this thermodynamic model, namely Na_2O, CaO, K_2O, FeO, MgO, Al_2O_3, SiO_2, H_2O, TiO_2 and O_2 (NCKFMASHTO). The thermodynamic models for solid solutions considered in the model are Melt(HGPH), St(W), Ctd(W), Ep(HP11), Fsp(C1), Gt(HGP), Opx(HGP), Cpx(HGP), Crd(HGP), Bi(HGP), Mica(W), cAmph(G), IlHm(A) and Sp(HGP). The majority of these solution models were defined empirically and experimentally for relatively mafic systems, and their use for reliably simulating the evolution of a system displaying the composition of an average silicified basalt remains questionable. However, in the absence of experimental data on a silica-rich thermodynamic system, we consider that these solution models are applicable for any compositional case including for the average silicified basalt, as previously done for a pelitic source (Mayne *et al.*, 2019).

The major element compositions considered by our model for the average silicified and for the average unaltered mafic sources were calculated from previously analysed compositions of such rocks in the 3.5-3.2 Ga Onverwacht Group (Lahaye *et al.*, 1995; Furnes *et al.*, 2012; Puchtel *et al.*, 2013; Schneider *et al.*, 2018) and are given in **Table S-4**. For the silicified mafic source, we considered the major element compositions of silicified basalts published by Hofmann and Harris (2008) for eight different sections of silicified mafic lithologies and our own data acquired for five other sections to calculate the major element composition of the average silicified basalts (accessible here https://commons.datacite.org/doi.org/10.25519/qxr1-9y88). The composition of each silicified rock was weighted with its volumetric representativeness to avoid compositional bias due to the over-representation of highly silicified basalts (SiO_2 > 85 wt. %) in the existing data set. The compositions of equilibrated liquids and abundance of phases equilibrated at different P-T conditions (along the 600 °C/GPa, 700 °C/GPa, 800 °C/GPa and 900 °C/GPa geotherms) are illustrated in **Fig. S-5** and **Fig. S-6**.

Modelling the O and Si isotopic compositions of the melts

The melt compositions and the proportion of co-existing mineral phases provided by the thermodynamic simulation were subsequently used to calculate the $\delta^{18}O$ and the $\delta^{30}Si$ of the melt along the four different P-T paths considered (i.e.

600 °C/GPa, 700 °C/GPa, 800 °C/GPa and 900 °C/GPa). This was done by considering the total isotopic composition of the closed system (i.e. the initial isotopic composition of starting materials), and the mineral/liquid fractionation of O and Si isotopes. For the starting average unaltered basalt composition, we considered a $\delta^{18}O$ and a $\delta^{30}Si$ composition of +5.6 ‰ and -0.29 ‰, respectively, which are typically representative of unaltered mantle-derived mafic to ultramafic rocks (Pack *et al.*, 2016; Savage *et al.*, 2010). For the silicified basalts, an average $\delta^{18}O$ value of +13 to +16 ‰ and an average $\delta^{30}Si$ of ~ +0.55 ‰ were calculated from the bulk-rock analyses published in the literature (Abraham *et al.*, 2011; de Wit & Furnes, 2016; Hofmann & Harris, 2008) for silicified lithologies from the Onverwacht. Most values of mineral/melt fractionation of O isotopes ($\Delta^{18}O_{mineral/melt}$) are for granitic systems and were calculated from the composition of bulk-rock samples and minerals published previously (Shieh and Schwarcz, 1974; Faure and Harris, 1991; Valley *et al.*, 1994; Lackey *et al.*, 2008; Fourie and Harris, 2011), whereas $\Delta^{30}Si_{mineral/melt}$ values were mainly calculated based on the dataset of Murphy *et al.* (2024). The value of $\Delta^{18}O_{pyroxene/melt}$ is not available in the compiled database and was therefore set to -0.5 ‰ based on the thermodynamic models of Bindeman *et al.* (2005) and Bucholz *et al.* (2017). Although $\Delta^{18}O_{mineral/melt}$ and $\Delta^{30}Si_{mineral/melt}$ should vary with thermodynamic conditions (i.e. P-T-X), we have fixed them to constant values provided in **Table S-4**. These values apply best for TTG melts as already argued by André *et al.* (2022) because they are based on isotopic analyses in natural migmatitic or granitic systems.

Considering the above parameters, the isotopic composition of the generated melt was calculated using a simple formula of Rayleigh distillation (André *et al.*, 2022):

$$\delta^x A_{ZRC} = \delta^x A_0 + 1000 \times (\alpha - 1) \times lnF$$

Where x is the mass number (30 or 18), A is an element (Si or O), F is the melting degree of the volume of melt in the system (at a considered P-T condition), $(\delta\,^xA)_0$ is the initial isotopic composition of the starting lithology (i.e. an average unaltered or silicified basalt) and α is an average coefficient of solid/liquid isotopic fractionation. Note that α is an average fractionation coefficient calculated as follows:

$$\alpha = \frac{\frac{\sum \Delta^x A_{mineral/melt} \times wt.\%_{mineral}}{\sum wt.\%_{mineral}}}{1000} + 1$$

Calculation of the O and Si isotopic composition of theoretical magmatic zircon

After calculating the O and Si isotopic composition of the melt produced at each P-T condition, we used empirically determined laws expressing $\delta^{18}O_{zircon}$ and $\delta^{30}Si_{zircon}$ as a function of melt compositions and system temperatures to estimate the isotopic composition of zircons that would have crystallised from the calculated melts. We used the following empirical laws respectively proposed by Lackey *et al.* (2008) and Guitreau *et al.* (2022) to calculate $\delta^{18}O_{zircon}$ and $\delta^{30}Si_{zircon}$ values:

$$\delta^{18}O_{zircon} = \delta^{18}O_{melt} - (0.0612 \times SiO_2 - 2.5)$$

and,

$$\delta^{30}Si_{zircon} = \delta^{30}Si_{melt} - (0.0054 \times \frac{10^6}{T^2} \times SiO_2)$$

where T is in Kelvin and SiO_2 represents the SiO_2 concentration in the liquid expressed in wt.%. Although zircon can precipitate at different temperatures and melt compositions during the evolution of a felsic melt, we simplified our calculation by considering that the average zircon precipitated at a temperature that was 50 °C lower than the initial melt temperature and that the composition of the melt remained unchanged until zircon crystallised. This might introduce a slight difference between the isotopic composition of zircon obtained in our model and the one that actually occurred in natural TTG systems, where zircon possibly precipitated continuously from a cooling and compositionally evolving melt. However, such differences are certainly comprised within analytical precision with which we typically measure the O and Si isotopic composition of natural zircons (i.e. 2 SD values <0.4 ‰). We therefore consider that our modelled zircon composition likely reflects (within error) that of zircons that could have precipitated from felsic melts produced by melting of either an average silicified basalt or an average unaltered basalt.

Supplementary Tables

Table S-1 Summary of O isotope, Si isotope and major element analyses (overleaf) in the BGGT TTG samples

Sample	TTG body	Type	Latitude	Longitude	$\delta^{18}O_{wr}$	$\delta^{18}O_{zrc}$	2SD	$\delta^{30}Si_{zrc}$	2SD	$\Delta^{18}O_{WR-Zrc}$
SK-KV01	Kaap Valley	Tonalite	-25.7702833	31.0655950		+5.7	0.4	-0.21	0.36	
SK-KV02	Kaap Valley	Trondhjemite	-25.8325333	30.8160167	+7.9					
SK-KV03	Kaap Valley	Trondhjemite	-25.8440667	30.8508000		+5.6	0.3	-0.33	0.28	
SK-KV04	Kaap Valley	Trondhjemite	-25.7178167	30.8422667		+5.4	0.3	-0.29	0.22	
SK-NL01	Nelshoogte	Trondhjemite	-25.8916833	30.6225500	+8.1					
SK-NL02	Nelshoogte	Trondhjemite	-25.8741333	30.6992333		+5.2	0.1	-0.57	0.50	
SK-NL03	Nelshoogte	Trondhjemite	-25.8153500	30.6447333		+5.8	1.0	-0.33	0.40	
SK-NL04	Nelshoogte	Tonalite	-25.7791000	30.6592667	+7.2	+5.6	0.8	-0.27	0.33	1.7
SK-THP03	Theespruit	Trondhjemite	-26.0559667	30.8503833	+7.4	+5.9	1.0	-0.37	0.49	1.5
SK-SLZ01	Stolzburg	Trondhjemite	-25.9079667	31.0906000	+6.9	+4.8	0.5	-0.60	0.50	2.1
SK-SLZ02	Stolzburg	Tonalite	-26.0247333	30.7619833	+7.2					

Table S-1 *Continued*

Sample	SiO_2	TiO_2	Al_2O_3	MgO	CaO	K_2O	Na_2O	Fe_2O_3	L.O.I.	Total
SK-KV01	63.6	0.5	15.3	3.0	4.8	1.3	4.3	5.2	1.9	99.9
SK-KV02	67.1	0.4	15.6	1.8	3.8	1.2	4.9	3.8	1.2	99.8
SK-KV03	67.3	0.5	15.1	2.0	3.6	1.1	4.9	4.2	1.6	100.2
SK-KV04	70.2	0.3	15.6	1.3	3.3	1.4	5.2	2.9	0.6	100.7
SK-NL01	72.8	0.3	15.1	0.6	2.9	1.1	4.9	2.3	0.7	100.6
SK-NL02	73.5	0.2	14.4	0.5	2.3	1.8	4.7	2.1	0.7	100.3
SK-NL03	70.0	0.4	15.2	1.3	3.3	1.0	4.8	3.2	1.1	100.3
SK-NL04	58.2	0.9	13.9	6.6	5.6	1.1	3.5	8.6	2.0	100.3
SK-THP03	72.2	0.3	15.0	1.0	2.5	1.4	5.4	2.3	0.6	100.6
SK-SLZ01	72.4	0.2	15.3	0.4	2.1	1.9	5.6	1.7	0.5	100.0
SK-SLZ02	60.1	1.0	18.4	2.2	5.2	1.6	5.7	4.8	1.4	100.4

Table S-2 SIMS analyses of O isotope compositions in Barberton TTG zircons and in 91500 standard zircon. $\delta^{18}O$, IMF and 2Se values are expressed in ‰.

Sample #	Ipr (nA)	$^{18}O/^{16}O$ H'2/L'2	16O/Coeff L'2	yield	$\delta^{18}O$raw	2se	IMF	**Corrected $\delta^{18}O$**	2se
91500_2	1.96E+00	2.03E-03	2.09E+09	1.07E+09	11.77	0.10	1.91	**10.09**	0.10
91500_3	1.96E+00	2.03E-03	2.08E+09	1.06E+09	11.84	0.12	1.98	**10.16**	0.12
91500_5	1.96E+00	2.03E-03	2.08E+09	1.07E+09	11.72	0.13	1.86	**10.04**	0.13
91500_6	1.95E+00	2.03E-03	2.08E+09	1.07E+09	11.54	0.10	1.68	**9.86**	0.10
91500_8	1.95E+00	2.03E-03	2.09E+09	1.07E+09	11.34	0.10	1.48	**9.66**	0.10
91500_9	1.95E+00	2.03E-03	2.08E+09	1.07E+09	11.46	0.12	1.60	**9.78**	0.12
91500_10	1.95E+00	2.03E-03	2.08E+09	1.07E+09	11.53	0.12	1.67	**9.85**	0.12
91500_11	1.94E+00	2.03E-03	2.08E+09	1.07E+09	11.41	0.12	1.55	**9.73**	0.12
91500_12	1.94E+00	2.03E-03	2.07E+09	1.07E+09	11.16	0.10	1.30	**9.48**	0.10
91500_14	1.94E+00	2.03E-03	2.07E+09	1.07E+09	11.53	0.12	1.67	**9.85**	0.12
91500_15	1.94E+00	2.03E-03	2.07E+09	1.07E+09	11.48	0.12	1.62	**9.80**	0.12
THP03-01_1	1.93E+00	2.02E-03	2.00E+09	1.03E+09	7.56	0.18		**5.86**	0.18
THP03-01_2	1.93E+00	2.02E-03	1.97E+09	1.02E+09	8.77	0.27		**7.08**	0.27
THP03-02_1	1.93E+00	2.02E-03	2.00E+09	1.03E+09	8.10	0.21		**6.40**	0.21
THP03-02_2	1.93E+00	2.03E-03	1.91E+09	9.91E+08	11.61	0.15		**9.91**	0.15
THP03-03_1	1.93E+00	2.02E-03	2.01E+09	1.04E+09	8.04	0.23		**6.34**	0.23
THP03-03_2	1.93E+00	2.02E-03	2.00E+09	1.04E+09	7.39	0.13		**5.69**	0.13
THP03-04_1	1.93E+00	2.02E-03	2.00E+09	1.04E+09	7.94	0.21		**6.24**	0.21
THP03-04_2	1.92E+00	2.02E-03	1.95E+09	1.01E+09	9.20	0.23		**7.50**	0.23
THP03-05_1	1.92E+00	2.02E-03	2.01E+09	1.04E+09	7.66	0.19		**5.96**	0.19
THP03-06_1	1.93E+00	2.02E-03	2.02E+09	1.05E+09	7.07	0.12		**5.38**	0.12
THP03-06_2	1.93E+00	2.02E-03	2.01E+09	1.04E+09	7.22	0.17		**5.53**	0.17
THP03-07_1	1.92E+00	2.02E-03	1.95E+09	1.01E+09	9.30	0.18		**7.60**	0.18
THP03-08_1	1.92E+00	2.02E-03	2.01E+09	1.04E+09	7.11	0.13		**5.41**	0.13
THP03-08_2	1.92E+00	2.02E-03	1.96E+09	1.02E+09	8.32	0.16		**6.63**	0.16
THP03-09_1	1.92E+00	2.02E-03	2.02E+09	1.05E+09	7.06	0.10		**5.37**	0.10
THP03-09_2	1.92E+00	2.02E-03	2.00E+09	1.04E+09	8.05	0.24		**6.36**	0.24
91500_17	1.92E+00	2.03E-03	2.04E+09	1.06E+09	11.86	0.12	2.00	**10.18**	0.12
THP03-10_1	1.92E+00	2.02E-03	1.99E+09	1.04E+09	8.00	0.20		**6.30**	0.20

Sample #	Ipr (nA)	$^{18}O/^{16}O$ H'2/L'2	16O/Coeff L'2	yield	$\delta^{18}O$raw	2se	IMF	**Corrected $\delta^{18}O$**	2se
THP03-10_2	1.92E+00	2.02E-03	1.99E+09	1.04E+09	7.21	0.13		**5.52**	0.13
THP03-11_1	1.92E+00	2.02E-03	1.99E+09	1.04E+09	8.38	0.18		**6.68**	0.18
THP03-11_2	1.92E+00	2.02E-03	1.96E+09	1.02E+09	9.16	0.14		**7.47**	0.14
THP03-13_1	1.92E+00	2.02E-03	2.01E+09	1.05E+09	7.05	0.13		**5.35**	0.13
NL03-01_1	1.92E+00	2.02E-03	2.01E+09	1.05E+09	7.07	0.12		**5.37**	0.12
NL03-01_2	1.92E+00	2.02E-03	2.00E+09	1.04E+09	9.24	0.18		**7.55**	0.18
NL03-02_1	1.92E+00	2.02E-03	1.99E+09	1.04E+09	7.44	0.17		**5.74**	0.17
91500_18	1.92E+00	2.03E-03	2.05E+09	1.07E+09	11.84	0.12	1.98	**10.16**	0.12
NL03-03_1	1.92E+00	2.02E-03	1.99E+09	1.04E+09	7.78	0.13		**6.09**	0.13
NL03-03_2	1.92E+00	2.02E-03	1.98E+09	1.03E+09	7.62	0.18		**5.92**	0.18
NL03-04_1	1.92E+00	2.02E-03	1.99E+09	1.04E+09	7.74	0.17		**6.05**	0.17
NL03-05_1	1.92E+00	2.02E-03	1.94E+09	1.01E+09	6.10	0.17		**4.40**	0.17
NL03-05_2	1.91E+00	2.02E-03	1.99E+09	1.04E+09	7.56	0.16		**5.87**	0.16
NL03-06_1	1.91E+00	2.02E-03	1.99E+09	1.04E+09	7.26	0.15		**5.56**	0.15
NL03-06_2	1.91E+00	2.02E-03	2.00E+09	1.05E+09	7.09	0.11		**5.39**	0.11
NL03-07_1	1.91E+00	2.02E-03	1.95E+09	1.02E+09	8.89	0.57		**7.20**	0.57
91500_19	1.91E+00	2.03E-03	2.03E+09	1.06E+09	11.49	0.10	1.63	**9.81**	0.10
NL03-10_1	1.91E+00	2.02E-03	1.99E+09	1.05E+09	7.34	0.13		**5.64**	0.13
NL03-10_2	1.90E+00	2.02E-03	1.97E+09	1.04E+09	7.71	0.14		**6.01**	0.14
NL03-11_1	1.90E+00	2.02E-03	1.97E+09	1.04E+09	7.28	0.13		**5.58**	0.13
NL03-12_1	1.90E+00	2.02E-03	1.96E+09	1.03E+09	8.10	0.18		**6.40**	0.18
NL03-12_2	1.90E+00	2.02E-03	1.97E+09	1.04E+09	7.49	0.14		**5.80**	0.14
NL03-15_1	1.90E+00	2.02E-03	1.98E+09	1.04E+09	7.06	0.13		**5.36**	0.13
NL03-15_2	1.90E+00	2.02E-03	1.98E+09	1.04E+09	6.99	0.10		**5.29**	0.10
NL03-17_1	1.90E+00	2.02E-03	1.99E+09	1.05E+09	7.16	0.11		**5.47**	0.11
91500_20	1.90E+00	2.03E-03	2.00E+09	1.05E+09	11.73	0.10	1.87	**10.05**	0.10
NL03-17_2	1.90E+00	2.02E-03	1.89E+09	9.92E+08	6.75	0.17		**5.05**	0.17
NL03-19_1	1.90E+00	2.02E-03	1.96E+09	1.03E+09	8.33	0.14		**6.63**	0.14
NL03-20_1	1.90E+00	2.02E-03	1.95E+09	1.03E+09	8.38	0.24		**6.68**	0.24
NL03-23_1	1.90E+00	2.02E-03	1.93E+09	1.02E+09	8.49	0.18		**6.79**	0.18
NL03-24_1	1.90E+00	2.02E-03	1.96E+09	1.03E+09	6.93	0.13		**5.23**	0.13
NL03-25_1	1.90E+00	2.02E-03	1.95E+09	1.03E+09	7.38	0.11		**5.68**	0.11
NL03-26_1	1.90E+00	2.02E-03	1.95E+09	1.03E+09	7.55	0.10		**5.85**	0.10
NL03-27_1	1.89E+00	2.02E-03	1.96E+09	1.04E+09	6.96	0.13		**5.27**	0.13
91500_21	1.89E+00	2.03E-03	2.00E+09	1.06E+09	11.66	0.11	1.80	**9.98**	0.11
91500_24	1.88E+00	2.03E-03	2.01E+09	1.07E+09	11.37	0.16	1.51	**9.69**	0.16
NL04-01_1	1.88E+00	2.02E-03	1.94E+09	1.03E+09	6.53	0.11		**4.84**	0.11
NL04-01_2	1.88E+00	2.02E-03	1.89E+09	1.01E+09	8.41	0.17		**6.72**	0.17
NL04-02_1	1.87E+00	2.02E-03	1.94E+09	1.04E+09	7.66	0.11		**5.97**	0.11
NL04-02_2	1.87E+00	2.02E-03	1.93E+09	1.03E+09	7.60	0.14		**5.90**	0.14
NL04-03_1	1.87E+00	2.02E-03	1.94E+09	1.04E+09	6.58	0.10		**4.88**	0.10
NL04-03_2	1.87E+00	2.02E-03	1.92E+09	1.03E+09	6.78	0.16		**5.08**	0.16
NL04-04_1	1.87E+00	2.02E-03	1.94E+09	1.04E+09	6.83	0.13		**5.13**	0.13
NL04-04_2	1.87E+00	2.02E-03	1.94E+09	1.04E+09	6.63	0.12		**4.94**	0.12
NL04-05_1	1.87E+00	2.02E-03	1.94E+09	1.04E+09	7.54	0.12		**5.84**	0.12
NL04-05_2	1.86E+00	2.02E-03	1.94E+09	1.04E+09	7.56	0.16		**5.87**	0.16
91500_25	1.86E+00	2.03E-03	1.99E+09	1.07E+09	11.39	0.15	1.53	**9.71**	0.15
NL04-07_1	1.86E+00	2.02E-03	1.92E+09	1.03E+09	8.04	0.22		**6.35**	0.22
NL04-07_2	1.86E+00	2.03E-03	1.94E+09	1.04E+09	9.68	0.30		**7.99**	0.30
NL04-08_1	1.86E+00	2.02E-03	1.92E+09	1.03E+09	7.04	0.12		**5.34**	0.12
NL04-08_2	1.86E+00	2.02E-03	1.94E+09	1.04E+09	7.41	0.16		**5.71**	0.16
NL04-09_1	1.85E+00	2.02E-03	1.93E+09	1.04E+09	7.31	0.12		**5.61**	0.12
NL04-10_1	1.85E+00	2.02E-03	1.92E+09	1.04E+09	7.02	0.14		**5.32**	0.14
NL04-11_1	1.85E+00	2.02E-03	1.92E+09	1.04E+09	6.93	0.12		**5.24**	0.12

Sample #	Ipr (nA)	$^{18}O/^{16}O$ H'2/L'2	16O/Coeff L'2	yield	$\delta^{18}O$raw	2se	IMF	**Corrected $\delta^{18}O$**	2se
NL04-11_2	1.85E+00	2.02E-03	1.92E+09	1.04E+09	7.14	0.15		**5.44**	0.15
NL04-12_1	1.85E+00	2.02E-03	1.93E+09	1.04E+09	7.37	0.13		**5.68**	0.13
NL04-13_1	1.85E+00	2.02E-03	1.95E+09	1.06E+09	7.09	0.10		**5.40**	0.10
91500_26	1.85E+00	2.03E-03	1.98E+09	1.07E+09	11.38	0.11	1.52	**9.70**	0.11
NL04-13_2	1.85E+00	2.02E-03	1.94E+09	1.05E+09	6.80	0.12		**5.11**	0.12
NL04-19_1	1.85E+00	2.02E-03	1.94E+09	1.05E+09	7.34	0.11		**5.64**	0.11
NL04-19_2	1.85E+00	2.02E-03	1.93E+09	1.05E+09	7.36	0.13		**5.66**	0.13
NL04-21_1	1.85E+00	2.02E-03	1.91E+09	1.04E+09	7.24	0.15		**5.54**	0.15
NL04-21_2	1.85E+00	2.02E-03	1.91E+09	1.04E+09	7.92	0.13		**6.22**	0.13
NL04-22_1	1.84E+00	2.02E-03	1.92E+09	1.04E+09	7.22	0.10		**5.53**	0.10
NL04-22_2	1.84E+00	2.02E-03	1.91E+09	1.04E+09	7.79	0.15		**6.09**	0.15
NL04-24_1	1.84E+00	2.02E-03	1.85E+09	1.00E+09	6.71	0.26		**5.01**	0.26
NL02-02_1	1.84E+00	2.02E-03	1.93E+09	1.05E+09	6.90	0.11		**5.20**	0.11
NL02-02_2	1.84E+00	2.02E-03	1.92E+09	1.04E+09	6.83	0.14		**5.13**	0.14
91500_27	1.84E+00	2.03E-03	1.98E+09	1.08E+09	11.34	0.16	1.48	**9.66**	0.16
KV04-01_1	1.84E+00	2.02E-03	1.92E+09	1.05E+09	7.32	0.10		**5.63**	0.10
KV04-01_2	1.84E+00	2.02E-03	1.90E+09	1.04E+09	7.19	0.10		**5.49**	0.10
KV04-02_1	1.84E+00	2.02E-03	1.91E+09	1.04E+09	7.21	0.13		**5.51**	0.13
KV04-02_2	1.84E+00	2.02E-03	1.92E+09	1.04E+09	6.95	0.12		**5.26**	0.12
KV04-03_1	1.83E+00	2.02E-03	1.89E+09	1.03E+09	6.97	0.12		**5.27**	0.12
KV04-03_2	1.83E+00	2.02E-03	1.90E+09	1.04E+09	7.19	0.11		**5.49**	0.11
KV01-03_1	1.83E+00	2.02E-03	1.93E+09	1.05E+09	7.20	0.10		**5.50**	0.10
KV01-04_1	1.83E+00	2.02E-03	1.93E+09	1.05E+09	7.31	0.14		**5.61**	0.14
KV01-04_2	1.83E+00	2.02E-03	1.93E+09	1.05E+09	8.03	0.15		**6.33**	0.15
KV01-05_1	1.83E+00	2.02E-03	1.93E+09	1.06E+09	7.33	0.11		**5.63**	0.11
91500_28	1.83E+00	2.03E-03	1.97E+09	1.08E+09	11.27	0.11	1.41	**9.59**	0.11
KV01-05_2	1.82E+00	2.02E-03	1.92E+09	1.05E+09	7.60	0.10		**5.91**	0.10
KV01-06_1	1.82E+00	2.02E-03	1.91E+09	1.05E+09	7.30	0.13		**5.60**	0.13
KV01-06_2	1.82E+00	2.02E-03	1.94E+09	1.07E+09	7.69	0.45		**6.00**	0.45
KV01-07_1	1.82E+00	2.02E-03	1.92E+09	1.05E+09	7.25	0.13		**5.55**	0.13
KV01-07_2	1.82E+00	2.02E-03	1.92E+09	1.05E+09	7.21	0.11		**5.52**	0.11
KV01-08_1	1.82E+00	2.02E-03	1.90E+09	1.04E+09	7.28	0.13		**5.58**	0.13
KV01-10_1	1.82E+00	2.02E-03	1.92E+09	1.05E+09	7.48	0.15		**5.78**	0.15
KV01-10_2	1.82E+00	2.02E-03	1.91E+09	1.05E+09	7.31	0.12		**5.62**	0.12
KV01-11_1	1.82E+00	2.02E-03	1.91E+09	1.05E+09	7.25	0.12		**5.55**	0.12
KV01-12_1	1.82E+00	2.02E-03	1.90E+09	1.05E+09	7.26	0.12		**5.56**	0.12
91500_29	1.82E+00	2.03E-03	1.94E+09	1.07E+09	11.48	0.12	1.62	**9.80**	0.12
KV01-12_2	1.82E+00	2.02E-03	1.89E+09	1.04E+09	7.62	0.12		**5.92**	0.12
91500_31	1.81E+00	2.03E-03	1.91E+09	1.06E+09	11.76	0.10	1.90	**10.08**	0.10
91500_32	1.81E+00	2.03E-03	1.91E+09	1.05E+09	11.67	0.14	1.81	**9.99**	0.14
KV01-14_2	1.81E+00	2.02E-03	1.78E+09	9.86E+08	6.78	0.23		**5.06**	0.23
KV01-16_1	1.80E+00	2.02E-03	1.89E+09	1.05E+09	7.27	0.10		**5.55**	0.10
KV01-16_2	1.80E+00	2.02E-03	1.87E+09	1.04E+09	7.50	0.12		**5.79**	0.12
KV01-24_1	1.80E+00	2.02E-03	1.87E+09	1.04E+09	7.57	0.11		**5.85**	0.11
KV01-24_2	1.80E+00	2.02E-03	1.86E+09	1.03E+09	7.35	0.12		**5.63**	0.12
KV03-01_1	1.80E+00	2.02E-03	1.89E+09	1.05E+09	7.46	0.11		**5.74**	0.11
KV03-01_2	1.80E+00	2.02E-03	1.90E+09	1.05E+09	7.07	0.13		**5.36**	0.13
91500_33	1.80E+00	2.03E-03	1.92E+09	1.07E+09	11.51	0.14	1.65	**9.83**	0.14
KV03-02_1	1.80E+00	2.02E-03	1.88E+09	1.05E+09	7.26	0.11		**5.54**	0.11
KV03-02_2	1.80E+00	2.02E-03	1.88E+09	1.05E+09	7.28	0.11		**5.57**	0.11
KV03-03_1	1.80E+00	2.02E-03	1.89E+09	1.05E+09	7.33	0.15		**5.62**	0.15
KV03-03_2	1.80E+00	2.02E-03	1.90E+09	1.06E+09	7.33	0.12		**5.62**	0.12
KV03-05_1	1.80E+00	2.02E-03	1.89E+09	1.05E+09	7.33	0.12		**5.62**	0.12
KV03-05_2	1.79E+00	2.02E-03	1.90E+09	1.06E+09	7.38	0.12		**5.66**	0.12

Sample #	Ipr (nA)	$^{18}O/^{16}O$ H'2/L'2	16O/Coeff L'2	yield	$\delta^{18}O$raw	2se	IMF	**Corrected $\delta^{18}O$**	2se
KV03-06_1	1.79E+00	2.02E-03	1.90E+09	1.06E+09	7.23	0.13		**5.51**	0.13
KV03-06_2	1.79E+00	2.02E-03	1.90E+09	1.06E+09	7.37	0.10		**5.65**	0.10
KV03-07_1	1.79E+00	2.02E-03	1.89E+09	1.05E+09	7.31	0.12		**5.59**	0.12
KV03-08_1	1.79E+00	2.02E-03	1.89E+09	1.06E+09	7.33	0.12		**5.61**	0.12
91500_34	1.79E+00	2.03E-03	1.90E+09	1.06E+09	11.57	0.10	1.71	**9.89**	0.10
KV03-09_1	1.79E+00	2.02E-03	1.86E+09	1.04E+09	8.06	0.22		**6.34**	0.22
KV03-10_1	1.79E+00	2.02E-03	1.88E+09	1.05E+09	7.11	0.14		**5.39**	0.14
KV03-11_1	1.79E+00	2.02E-03	1.87E+09	1.04E+09	7.32	0.10		**5.60**	0.10
KV03-14_1	1.78E+00	2.02E-03	1.88E+09	1.05E+09	7.45	0.14		**5.73**	0.14
KV03-14_2	1.78E+00	2.02E-03	1.86E+09	1.05E+09	7.13	0.14		**5.42**	0.14
KV03-15_1	1.78E+00	2.02E-03	1.84E+09	1.03E+09	6.87	0.17		**5.15**	0.17
KV03-16_1	1.78E+00	2.02E-03	1.87E+09	1.05E+09	7.38	0.13		**5.66**	0.13
KV03-17_1	1.78E+00	2.02E-03	1.86E+09	1.05E+09	7.21	0.10		**5.50**	0.10
KV03-17_2	1.78E+00	2.02E-03	1.86E+09	1.05E+09	7.20	0.12		**5.48**	0.12
KV03-18_1	1.78E+00	2.02E-03	1.86E+09	1.05E+09	7.02	0.12		**5.30**	0.12
91500_35	1.78E+00	2.03E-03	1.89E+09	1.07E+09	11.61	0.10	1.75	**9.93**	0.10
KV03-18_2	1.78E+00	2.02E-03	1.86E+09	1.05E+09	7.70	0.18		**5.98**	0.18
KV03-21_1	1.78E+00	2.02E-03	1.86E+09	1.05E+09	7.46	0.10		**5.74**	0.10
KV03-21_2	1.78E+00	2.02E-03	1.86E+09	1.05E+09	7.15	0.14		**5.44**	0.14
SLZ01-01_1	1.77E+00	2.02E-03	1.85E+09	1.04E+09	6.81	0.20		**5.09**	0.20
SLZ01-01_2	1.77E+00	2.02E-03	1.86E+09	1.05E+09	6.70	0.12		**4.98**	0.12
SLZ01-02_1	1.77E+00	2.02E-03	1.87E+09	1.05E+09	6.85	0.12		**5.13**	0.12
SLZ01-02_2	1.77E+00	2.02E-03	1.84E+09	1.04E+09	6.09	0.12		**4.37**	0.12
SLZ01-03_1	1.77E+00	2.02E-03	1.85E+09	1.05E+09	6.50	0.14		**4.78**	0.14
SLZ01-03_2	1.77E+00	2.02E-03	1.85E+09	1.05E+09	6.57	0.14		**4.85**	0.14
SLZ01-05_1	1.77E+00	2.02E-03	1.87E+09	1.06E+09	6.10	0.13		**4.38**	0.13
91500_36	1.77E+00	2.03E-03	1.87E+09	1.06E+09	11.45	0.13	1.59	**9.77**	0.13
SLZ01-05_2	1.77E+00	2.02E-03	1.86E+09	1.05E+09	6.67	0.16		**4.95**	0.16
SLZ01-06_1	1.77E+00	2.02E-03	1.85E+09	1.05E+09	6.56	0.12		**4.84**	0.12
SLZ01-06_2	1.77E+00	2.02E-03	1.85E+09	1.05E+09	6.23	0.10		**4.51**	0.10
SLZ01-08_1	1.76E+00	2.02E-03	1.85E+09	1.05E+09	6.49	0.10		**4.77**	0.10
SLZ01-08_2	1.76E+00	2.02E-03	1.86E+09	1.05E+09	6.52	0.13		**4.80**	0.13
SLZ01-10_1	1.76E+00	2.01E-03	1.84E+09	1.04E+09	2.83	0.19		**1.12**	0.19
SLZ01-14_1	1.76E+00	2.02E-03	1.84E+09	1.04E+09	6.38	0.15		**4.66**	0.15
SLZ01-15_1	1.76E+00	2.02E-03	1.85E+09	1.05E+09	6.52	0.15		**4.80**	0.15
SLZ01-15_2	1.76E+00	2.02E-03	1.84E+09	1.05E+09	6.86	0.11		**5.14**	0.11
SLZ01-16_1	1.76E+00	2.02E-03	1.84E+09	1.05E+09	6.66	0.12			0.12
91500_37	1.76E+00	2.03E-03	1.86E+09	1.06E+09	11.46	0.14	1.60	**9.78**	0.14
SLZ01-16_2	1.76E+00	2.02E-03	1.83E+09	1.04E+09	6.85	0.14		**5.13**	0.14
SLZ01-18_1	1.76E+00	2.02E-03	1.83E+09	1.04E+09	6.33	0.12		**4.61**	0.12
SLZ01-18_2	1.76E+00	2.02E-03	1.84E+09	1.05E+09	5.07	0.14		**3.36**	0.14
SLZ01-21_1	1.75E+00	2.02E-03	1.84E+09	1.05E+09	5.77	0.17		**4.05**	0.17
SLZ01-21_2	1.75E+00	2.02E-03	1.83E+09	1.04E+09	5.02	0.16		**3.31**	0.16
Average 91500								**9.86±0.36 (2SD)**	

Grey lines are standard analyses. In red are data that were excluded due to significant shift from the magmatic value measured in other grains. These data are based on spots located in fractured zones (see images on Figure S-2). The shift from isotopic compositions obtained from non-fractured spots is likely due to alteration of analysed zircon areas, which is not discussed in this manuscript.

Table S-3 LA-MC-ICP-MS analysis of Si isotope compositions in zircon. Errors, $\delta^{29}Si$, and $\delta^{30}Si$ values are expressed in ‰.

Name	$\delta^{29}Si$	2 σ	$\delta^{30}Si$	2 σ	^{28}Si (V)	$^{27}Al/^{28}Si$	$\delta^{30}Si'$ from $\delta^{29}Si$	2 σ
Natural zircons								
SLZ01-01b	-0.30	0.11	**-0.53**	**0.30**	6.39	0.0009	-0.57	0.11
SLZ01-01a	-0.35	0.11	**-0.56**	**0.34**	5.95	0.0011	-0.67	0.11
SLZ01-02b	-0.50	0.12	**-0.85**	**0.15**	5.93	0.0022	-0.96	0.12
SLZ01-02a	-0.37	0.12	**-0.41**	**0.20**	5.55	0.0029	-0.72	0.12
SLZ01-03b	-0.31	0.11	**-0.75**	**0.15**	5.17	0.0026	-0.59	0.11
SLZ01-03a	-0.18	0.13	**-0.39**	**0.20**	5.32	0.0086	-0.35	0.13
SLZ01-05b	-0.26	0.12	**-0.70**	**0.23**	5.51	0.0014	-0.50	0.12
SLZ01-05a	-0.37	0.15	**-0.76**	**0.14**	4.15	0.0000	-0.71	0.15
SLZ01-06b	-0.27	0.14	**-0.63**	**0.23**	4.10	0.0024	-0.51	0.14
SLZ01-06a	-0.23	0.13	**-0.59**	**0.37**	5.38	0.0032	-0.45	0.13
SLZ01-08b	-0.37	0.14	**-0.12**	**0.21**	5.05	0.0034	-0.72	0.14
SLZ01-08a	-0.59	0.13	**-0.53**	**0.25**	4.83	0.0132	-1.15	0.13
SLZ01-10	-0.54	0.21	**-1.07**	**0.39**	4.48	0.0160	-1.05	0.21
SLZ01-14	-0.39	0.12	**-1.00**	**0.36**	5.30	0.0031	-0.76	0.12
SLZ01-15	-0.42	0.13	**-0.41**	**0.16**	4.79	0.0017	-0.80	0.13
SLZ01-18b	-0.34	0.14	**-0.34**	**0.19**	4.54	0.0018	-0.65	0.14
Average SLZ01			**-0.55**	**0.39**				
KV03-01a	-0.27	0.11	**-0.43**	**0.22**	5.96	0.0000	-0.53	0.11
KV03-02	-0.23	0.12	**-0.32**	**0.20**	5.28	0.0001	-0.43	0.12
KV03-03	-0.32	0.14	**-0.04**	**0.25**	5.18	0.0000	-0.61	0.14
KV03-05a	-0.31	0.11	**-0.46**	**0.20**	5.90	0.0000	-0.59	0.11
KV03-06	-0.07	0.17	**-0.37**	**0.24**	6.30	0.0000	-0.13	0.17
KV03-07	-0.15	0.12	**-0.40**	**0.22**	5.17	0.0001	-0.28	0.12
KV03-08	-0.29	0.11	**-0.30**	**0.21**	5.83	0.0000	-0.56	0.11
Average KV03			**-0.33**	**0.28**				
NL02bout	-0.34	0.11	**-0.39**	**0.35**	5.68	0.0014	-0.66	0.11
NL02coeur	-0.29	0.12	**-0.75**	**0.40**	5.83	0.0791	-0.57	0.12
Average NL02			**-0.39**	**0.35**				
KV04-01a	-0.24	0.11	**-0.13**	**0.42**	5.89	0.0001	-0.46	0.11
KV04-01b	-0.49	0.13	**-0.25**	**0.42**	6.44	0.0003	-0.94	0.13
KV04-02a	-0.29	0.12	**-0.24**	**0.32**	5.78	0.0030	-0.55	0.12
KV04-02b	-0.52	0.11	**-0.25**	**0.25**	5.86	0.0087	-1.00	0.11
KV04-3a	-0.26	0.12	**-0.42**	**0.41**	5.61	0.0013	-0.50	0.12
KV04-03b	-0.19	0.12	**-0.42**	**0.39**	5.79	0.0021	-0.37	0.12
Average KV04			**-0.29**	**0.22**				
KV01-03	-0.38	0.12	**-0.39**	**0.44**	5.43	0.0012	-0.73	0.12
KV01-04b	-0.16	0.12	**-0.22**	**0.22**	5.91	0.0000	-0.30	0.12
KV01-04a	-0.23	0.16	**-0.05**	**0.36**	5.93	0.0001	-0.43	0.16
KV01-05a	-0.08	0.12	**0.00**	**0.28**	5.43	0.0000	-0.16	0.12
KV01-06a	-0.22	0.13	**-0.29**	**0.34**	5.37	0.0000	-0.43	0.13
KV01-07	-0.20	0.11	**-0.06**	**0.37**	5.45	0.0001	-0.38	0.11
KV01-14	-0.19	0.12	**-0.46**	**0.25**	5.39	0.0000	-0.37	0.12

Name	$\delta^{29}Si$	2 σ	$\delta^{30}Si$	2 σ	^{28}Si (V)	$^{27}Al/^{28}Si$	$\delta^{30}Si'$ from $\delta^{29}Si$	2 σ
Average KV01			**-0.17**	**0.31**				
NL04-1b	-0.29	0.12	**-0.25**	**0.31**	5.32	0.0011	-0.56	0.12
NL04-01a	-0.36	0.12	**-0.58**	**0.29**	5.08	0.0007	-0.69	0.12
NL04-2b	-0.30	0.11	**-0.31**	**0.23**	5.37	0.0002	-0.58	0.11
NL04-3	-0.16	0.12	**-0.06**	**0.35**	5.17	0.0000	-0.30	0.12
NL04-4a	-0.17	0.13	**-0.30**	**0.39**	5.62	0.0001	-0.32	0.13
NL04-5b	-0.16	0.13	**-0.16**	**0.33**	5.61	0.0002	-0.31	0.13
NL04-7a	-0.29	0.12	**-0.23**	**0.46**	5.63	0.0000	-0.55	0.12
Average NL04			**-0.27**	**0.15**				
THP03-5	-0.36	0.14	**-0.79**	**0.39**	5.57	0.0004	-0.70	0.14
THP03-06a	-0.18	0.14	**-0.30**	**0.47**	5.56	0.0000	-0.34	0.14
THP03-07	-0.31	0.15	**-0.34**	**0.55**	4.98	0.0016	-0.59	0.15
THP03-08a	-0.20	0.12	**-0.19**	**0.49**	5.53	0.0003	-0.39	0.12
THP03-9b	-0.22	0.12	**-0.21**	**0.53**	5.41	0.0006	-0.43	0.12
Average THP03			**-0.37**	**0.49**				
NL03-02b	-0.19	0.13	**-0.39**	**0.46**	5.49	0.0039	-0.36	0.13
NL03-04	-0.28	0.14	**-0.19**	**0.42**	5.64	0.0001	-0.54	0.14
NL03-05 (entre a-b)	-0.33	0.18	**-0.28**	**0.49**	5.84	0.0009	-0.63	0.18
NL03-6b	-0.60	0.13	**-0.14**	**0.50**	5.57	0.0001	-1.15	0.13
NL03-12	-0.50	0.19	**-0.64**	**0.56**	5.27	0.0068	-0.97	0.19
Average NL03			**-0.33**	**0.40**				
Standards								
Seq1-MudTank1	-0.05	0.11	**-0.21**	**0.19**	6.38	0.0000	-0.11	0.11
seq1-MudTank-2	-0.10	0.11	**-0.39**	**0.17**	4.82	0.0000	-0.19	0.11
seq2-MudTank-1	-0.26	0.12	**-0.21**	**0.14**	5.43	0.0000	-0.51	0.12
seq2-MudTank-2	-0.23	0.12	**-0.47**	**0.21**	5.11	0.0000	-0.44	0.12
seq2-MudTank-3	-0.19	0.13	**-0.32**	**0.17**	4.97	0.0000	-0.37	0.13
seq3-MudTank-1	-0.25	0.12	**-0.36**	**0.17**	5.60	0.0000	-0.47	0.12
seq3-MudTank-2	-0.11	0.11	**-0.60**	**0.23**	5.53	-0.0076	-0.21	0.11
Seq4_MudTank1	-0.03	0.12	**-0.44**	**0.28**	5.51	0.0000	-0.05	0.12
seq4-MudTank-2	-0.20	0.12	**-0.59**	**0.27**	5.30	0.0000	-0.39	0.12
seq4-MudTank-3	-0.32	0.12	**-0.28**	**0.31**	5.24	0.0000	-0.62	0.12
seq4-MudTank-4	-0.26	0.13	**-0.50**	**0.25**	4.93	0.0000	-0.51	0.13
seq5-MudTank-1	-0.17	0.12	**-0.30**	**0.66**	5.22	0.0000	-0.33	0.12
Seq5-MudTank-2	-0.18	0.13	**-0.58**	**0.47**	5.25	0.0000	-0.36	0.13
Average MudTank	**-0.18**	**0.18**	**-0.40**	**0.28**				
Seq1-MUN1	-0.93	0.10	**-2.27**	**0.28**	6.36	0.0003	-1.80	0.10
seq1-MUN2	-0.90	0.11	**-2.01**	**0.21**	5.01	0.0003	-1.74	0.11
seq-2-MUN-1	-1.10	0.12	**-2.48**	**0.15**	5.62	0.0004	-2.12	0.12
seq2-MUN-2	-0.96	0.13	**-1.85**	**0.19**	4.47	0.0004	-1.85	0.13
seq2-MUN-3	-0.95	0.13	**-2.09**	**0.18**	5.20	0.0003	-1.83	0.13
seq3-MUN-1	-0.93	0.11	**-1.68**	**0.21**	5.84	0.0001	-1.79	0.11
seq3-MUN-2	-0.99	0.13	**-1.94**	**0.24**	5.63	0.0001	-1.91	0.13
Seq4-MUN-1	-0.74	0.12	**-1.80**	**0.29**	5.68	0.0002	-1.43	0.12
seq4-MUN-2	-0.92	0.12	**-1.61**	**0.50**	5.48	0.0003	-1.78	0.12
seq4-MUN-3	-1.00	0.12	**-1.62**	**0.30**	5.28	0.0003	-1.94	0.12
seq4-MUN-4	-0.99	0.13	**-1.95**	**0.28**	4.92	0.0003	-1.91	0.13
seq5-MUN-1	-1.02	0.12	**-2.07**	**0.72**	5.41	0.0004	-1.97	0.12
seq5-MUN-2	-1.00	0.11	**-2.10**	**0.39**	5.33	0.0004	-1.93	0.11

Name	$\delta^{29}Si$	2 σ	$\delta^{30}Si$	2 σ	^{28}Si (V)	$^{27}Al/^{28}Si$	$\delta^{30}Si'$ from $\delta^{29}Si$	2 σ
Average MUN	**-0.96**	**0.16**	**-1.96**	**0.50**				
seq1-91500-2	-0.27	0.11	**-0.48**	**0.17**	6.67	0.0003	-0.49	0.11
Seq1-91500-3	-0.32	0.10	**-0.56**	**0.32**	6.46	0.0002	-0.57	0.10
seq1-91500-4	-0.13	0.11	**-0.20**	**0.30**	6.18	0.0003	-0.23	0.11
seq1-91500-5	-0.25	0.12	**-0.53**	**0.31**	6.01	0.0004	-0.44	0.12
seq1-91500-6	-0.17	0.12	**-0.20**	**0.17**	5.79	0.0002	-0.30	0.12
seq1-91500-7	-0.19	0.12	**-0.35**	**0.17**	5.50	0.0003	-0.36	0.12
seq1-91500-8	-0.19	0.11	**-0.38**	**0.16**	5.22	0.0003	-0.36	0.11
seq1-91500-9	-0.21	0.11	**-0.25**	**0.15**	5.09	0.0002	-0.41	0.11
seq2-91500-2	-0.13	0.12	**-0.29**	**0.15**	5.62	0.0003	-0.24	0.12
seq2-91500-3	-0.31	0.11	**-0.55**	**0.18**	5.73	0.0003	-0.60	0.11
seq2-91500-4	-0.17	0.11	**-0.12**	**0.17**	5.65	0.0006	-0.34	0.11
seq1-91500-5	-0.21	0.11	**-0.54**	**0.17**	5.55	0.0002	-0.41	0.11
seq2-91500-6	-0.20	0.13	**-0.30**	**0.18**	5.54	0.0003	-0.39	0.13
seq2-91500-7	-0.17	0.13	**-0.17**	**0.18**	5.54	0.0003	-0.32	0.13
Seq2-91500-8	-0.26	0.13	**-0.58**	**0.21**	5.50	0.0002	-0.50	0.13
seq-291500-9	-0.13	0.12	**-0.14**	**0.18**	5.46	0.0002	-0.25	0.12
seq2-91500-10	-0.26	0.12	**-0.54**	**0.22**	5.40	0.0001	-0.50	0.12
seq2-91500-11	-0.16	0.13	**-0.48**	**0.22**	5.41	0.0002	-0.32	0.13
seq2-91500-12	-0.24	0.13	**-0.32**	**0.39**	5.37	0.0002	-0.45	0.13
seq2-91500-13	-0.15	0.13	**-0.24**	**0.37**	5.43	0.0002	-0.30	0.13
seq2-91500-14	-0.25	0.12	**-0.36**	**0.36**	5.41	0.0004	-0.49	0.12
seq2-91500-15	-0.13	0.12	**-0.36**	**0.15**	5.32	0.0006	-0.26	0.12
seq2-91500-16	-0.25	0.12	**-0.56**	**0.16**	5.24	0.0002	-0.49	0.12
seq2-91500-17	-0.25	0.12	**-0.32**	**0.18**	5.26	0.0004	-0.48	0.12
seq3-91500-2	-0.25	0.12	**-0.27**	**0.21**	5.93	0.0004	-0.44	0.12
seq3-91500-3	-0.17	0.11	**-0.14**	**0.21**	5.94	0.0002	-0.30	0.11
seq3-91500-4	-0.18	0.12	**-0.45**	**0.19**	5.98	0.0003	-0.33	0.12
seq3-91500-5	-0.26	0.12	**-0.37**	**0.15**	5.97	0.0004	-0.47	0.12
seq3-91500-6	-0.09	0.12	**-0.45**	**0.18**	5.81	0.0003	-0.16	0.12
seq3-91500-7	-0.25	0.12	**-0.34**	**0.22**	5.86	0.0002	-0.48	0.12
seq3-91500-8	-0.28	0.11	**-0.42**	**0.24**	5.90	0.0003	-0.54	0.11
seq3-91500-9	-0.12	0.11	**-0.22**	**0.24**	5.92	-0.0068	-0.23	0.11
seq3-91500-10	-0.25	0.12	**-0.46**	**0.25**	5.84	-0.0069	-0.47	0.12
seq3-91500-11	-0.20	0.12	**-0.19**	**0.23**	5.80	-0.0070	-0.38	0.12
seq4-91500-2	-0.28	0.12	**-0.56**	**0.31**	5.81	0.0003	-0.50	0.12
seq4-91500-3	-0.20	0.12	**-0.26**	**0.33**	5.81	0.0003	-0.36	0.12
seq4-91500-4	-0.19	0.11	**-0.19**	**0.41**	5.78	0.0003	-0.33	0.11
seq4-91500-5	-0.21	0.11	**-0.45**	**0.41**	5.74	0.0002	-0.37	0.11
seq4-91500-6	-0.14	0.12	**-0.40**	**0.38**	5.67	0.0003	-0.26	0.12
seq4-91500-7	-0.23	0.12	**-0.31**	**0.29**	5.77	0.0001	-0.44	0.12
seq4-91500-8	-0.19	0.12	**-0.50**	**0.27**	5.63	0.0003	-0.37	0.12
seq4-91500-9	-0.19	0.11	**-0.39**	**0.26**	5.60	0.0002	-0.36	0.11
seq4-91500-10	-0.22	0.11	**-0.16**	**0.41**	5.74	0.0002	-0.42	0.11
seq4-91500-11	-0.23	0.12	**-0.38**	**0.41**	5.67	0.0002	-0.44	0.12
seq4-91500-12	-0.21	0.12	**-0.54**	**0.48**	5.66	0.0001	-0.41	0.12
seq4-91500-13	-0.18	0.12	**-0.22**	**0.37**	5.57	0.0002	-0.34	0.12
seq4-91500-14	-0.18	0.12	**-0.26**	**0.35**	5.57	0.0006	-0.34	0.12
seq4-91500-15	-0.20	0.12	**-0.56**	**0.25**	5.55	0.0004	-0.39	0.12
seq4-91500-16	-0.23	0.12	**-0.25**	**0.27**	5.55	0.0002	-0.45	0.12
seq4-91500-17	-0.18	0.12	**-0.36**	**0.27**	5.51	0.0003	-0.35	0.12
seq4-91500-18	-0.19	0.13	**-0.41**	**0.27**	5.52	0.0003	-0.38	0.13
seq4-91500-19	-0.22	0.13	**-0.36**	**0.28**	5.51	0.0003	-0.42	0.13
seq4-91500-20	-0.15	0.12	**-0.33**	**0.29**	5.52	0.0002	-0.28	0.12

Name	$\delta^{29}Si$	2 σ	$\delta^{30}Si$	2 σ	^{28}Si (V)	$^{27}Al/^{28}Si$	$\delta^{30}Si'$ from $\delta^{29}Si$	2 σ
sea4-91500-21	-0.22	0.12	**-0.33**	**0.28**	5.50	0.0002	-0.42	0.12
seq4-91500-22	-0.20	0.11	**-0.30**	**0.27**	5.42	0.0003	-0.38	0.11
seq4-91500-23	-0.29	0.11	**-0.35**	**0.26**	5.38	0.0002	-0.55	0.11
seq4-91500-24	-0.14	0.11	**-0.40**	**0.27**	5.39	0.0003	-0.27	0.11
seq4-91500-25	-0.12	0.12	**-0.41**	**0.26**	5.32	0.0003	-0.23	0.12
seq4-91500-26	-0.27	0.12	**-0.18**	**0.25**	5.20	0.0002	-0.51	0.12
seq4-91500-27	-0.19	0.12	**-0.49**	**0.25**	5.21	0.0002	-0.36	0.12
seq5-91500-2	-0.23	0.13	**-0.28**	**0.38**	5.46	0.0003	-0.41	0.13
seq5-91500-3	-0.13	0.13	**-0.13**	**0.31**	5.52	0.0006	-0.23	0.13
seq5-91500-4	-0.29	0.13	**-0.65**	**0.31**	5.60	0.0003	-0.52	0.13
seq91500-5	-0.18	0.12	**-0.34**	**0.38**	5.55	0.0003	-0.33	0.12
seq5-91500-6	-0.15	0.13	**-0.36**	**0.43**	5.47	0.0003	-0.27	0.13
seq5-91500-7	-0.16	0.14	**-0.45**	**0.46**	5.42	0.0003	-0.30	0.14
seq5-91500-8	-0.32	0.14	**-0.23**	**0.45**	5.43	0.0003	-0.62	0.14
seq5-91500-9	-0.09	0.13	**-0.25**	**0.48**	5.58	0.0003	-0.18	0.13
seq5-91500-10	-0.30	0.12	**-0.55**	**0.38**	5.45	0.0002	-0.59	0.12
seq5-91500-11	-0.10	0.11	**-0.39**	**0.45**	5.65	0.0004	-0.19	0.11
seq5-91500-12	-0.24	0.12	**-0.33**	**0.49**	5.45	0.0003	-0.46	0.12
seq5-91500-13	-0.20	0.12	**-0.30**	**0.53**	5.47	0.0003	-0.39	0.12
seq5-91500-14	-0.26	0.14	**-0.25**	**0.45**	5.41	0.0004	-0.51	0.14
seq5-91500-15	-0.15	0.14	**-0.45**	**0.41**	5.39	0.0003	-0.29	0.14
seq5-91500-16	-0.22	0.14	**-0.35**	**0.46**	5.39	0.0003	-0.43	0.14
seq5-91500-17	-0.13	0.12	**-0.32**	**0.50**	5.43	0.0003	-0.25	0.12
seq5-91500-18	-0.24	0.11	**-0.40**	**0.43**	5.33	0.0002	-0.46	0.11
Average 91500	**-0.20**	**0.11**	**-0.36**	**0.25**				

In red are data that were excluded due to significant shift from the magmatic value measured in other grains. These data are based on spots located in fractured zones (see images on Figure S-2). The shift from isotopic compositions obtained from non-fractured spots is likely due to alteration of analysed zircon areas, which is not discussed in this manuscript.

Table S-4 Parameters used in the thermodynamic model

Starting source compositions (wt.% and ‰)		
Lithology	Silicified basalt*	Unaltered basalt**
SiO_2	74.24	51.27
TiO_2	0.83	0.88
Fe_2O_3	7.82	11.98
FeO	7.03	10.78
Al_2O_3	7.15	12.37
MgO	2.44	9.54
CaO	1.44	7.85
Na_2O	0.42	2.60
K_2O	2.05	0.30
H_2O	3.10	4.59
O_2	0.18	0.18
$\delta^{18}O$	+10 to +15 ‰	+5.6 ‰
$\delta^{30}Si$	+0.55 ‰	-0.29 ‰

Mineral-melt fractionation coefficients***		
Phase	$\Delta^{30}Si_{mineral\text{-}melt}$	$\Delta^{18}O_{mineral\text{-}melt}$
Quartz	+0.04	+1.8
Plagioclase	-0.08	-0.1
Alkali feldspar		-0.1
Amphibole	-0.38	-2.9
Biotite		-4.0
Pyroxene	-0.33	-0.5
Garnet	-0.47	-2.8
magnetite		-7.1

*The major compositions of silicified basaltic source from the Barberton Greenstone Belt are based on published dataset of (Hofmann and Harris, 2008) complemented by our own dataset (accessible here https://commons.datacite.org/doi.org/10.25519/qxr1-9y88). The considered O and Si isotopic composition of this source are based on previously published compositions of silicified lavas from the Onverwacht Group (Hofmann and Harris, 2008; Abraham *et al.*, 2011; Kitoga *et al.*, 2024).

**The major element compositions of unaltered basalts used in our model were calculated based on previously published representative compositions of Barberton (Onverwacht) mafic rocks (Lahaye *et al.*, 1995; Furnes *et al., 2012;* Puchtel *et al.,* 2013*;* Schneider *et al.,* 2019*)*. The O and Si isotope compositions of unaltered basalts are considered identical to typical fresh mantle-derived lavas(Savage *et al.*, 2010; Pack and Herwartz, 2014;).

***Mineral melt fractionation coefficients of Si isotopes ($\Delta^{30}Si_{mineral\text{-}melt}$) were calculated based on Si isotope compositions of different phases in an Archean granulite (Murphy *et al.*, 2024). Mineral-melt fractionations ($\Delta^{18}O_{mineral\text{-}melt}$) of O isotopes were based on a compilation of different phase composition in magmatic systems (Shieh and Schwarcz, 1974; Faure and Harris, 1991; Lackey et al., 2008; Valley *et al.*, 1994; Fourie and Harris, 2011;). The pyroxyene-liquid fractionation of O isotopes was taken from (Bindeman *et al.*, 2005) and is consistent with values obtained by numerical calculations of (Bucholz *et al.*, 2017)

Table S-5 References for O and Si isotopic compositions of magmatic zircons older than 3.0 Ga compiled from the literature and represented by density curves in Figure 3.

O isotope compositions of Pre-3.0 Ga magmatic zircons	Si isotope compositions of Pre-3.0 Ga magmatic zircons
• Bell *et al.*, 2011; • Bell and Harrison, 2013; • **Chowdhury *et al.*, 2021, 2023;** • Hiess *et al.*, 2011; • **Lei *et al.*, 2023;** • Roberts & Santosh, 2018; • Smithies *et al.*, 2021; • **Trail *et al.*, 2018;** • Valley *et al.*, 2005; • Vezinet *et al.*, 2018, 2019; • Wang *et al.*, 2022; • Zeh *et al.*, 2014	• **Chowdhury *et al.*, 2021, 2023;** • Guitreau *et al.*, 2022; • **Lei *et al.*, 2023;** • **Trail *et al.*, 2018**

In bold are papers that reported both O and Si isotopic compositions of zircon.

Supplementary Figures

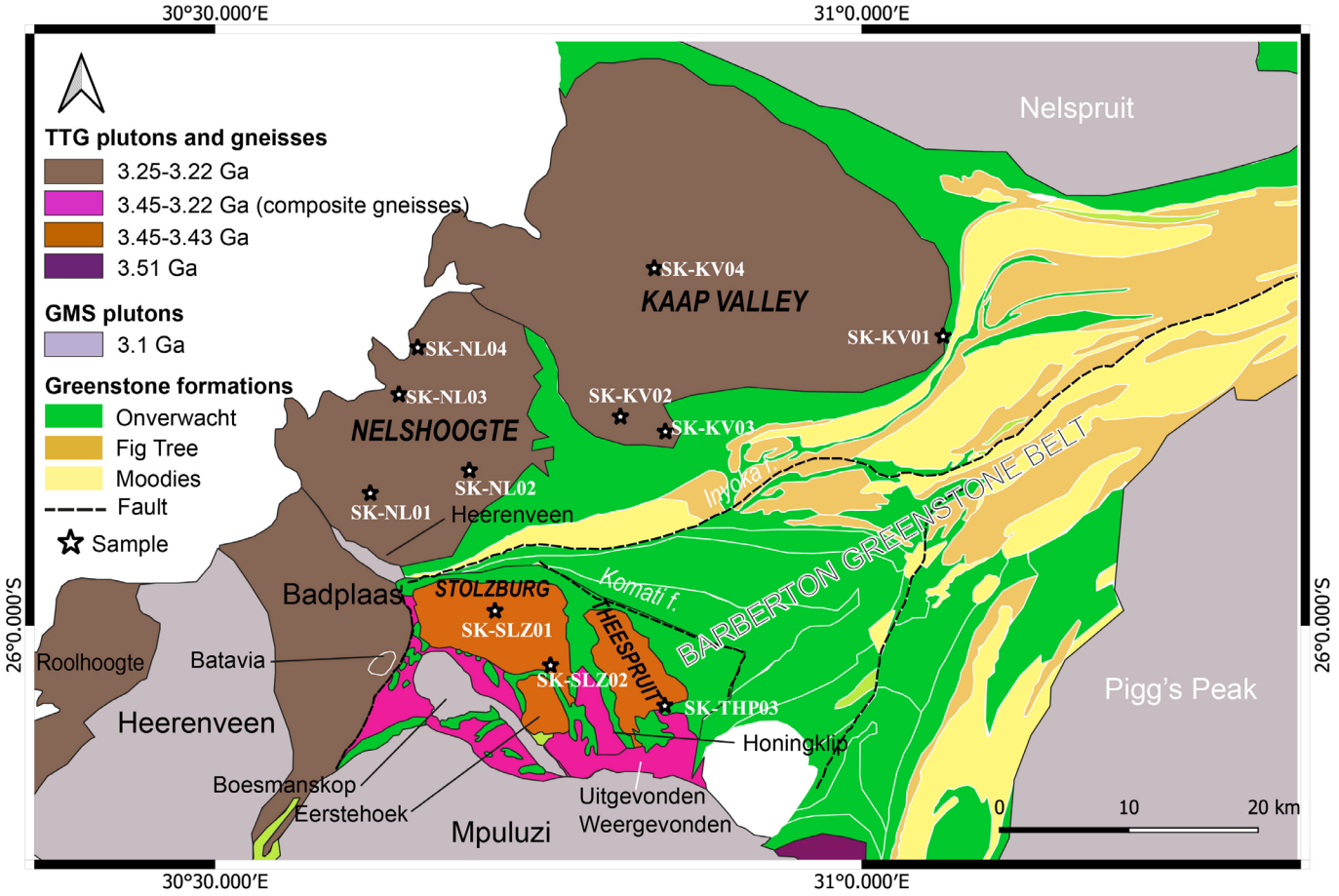

Figure S-1 Simplified geological map of the Barberton Granitoid-Greenstone Terrain. The location of outcrops from which the eleven samples analysed in this study were collected is represented with stars. The names of plutons for which isotopic compositions are discussed in this study are written in upper case and among these, the names of plutons for which we produced new data are in capital letter. The unmapped white body near Steynsdorp represents a younger granitoid. Abbreviations: TTG = tonalite-trondhjemite-granodiorite series and GMS = Granite-Monzonite-Syenite series.

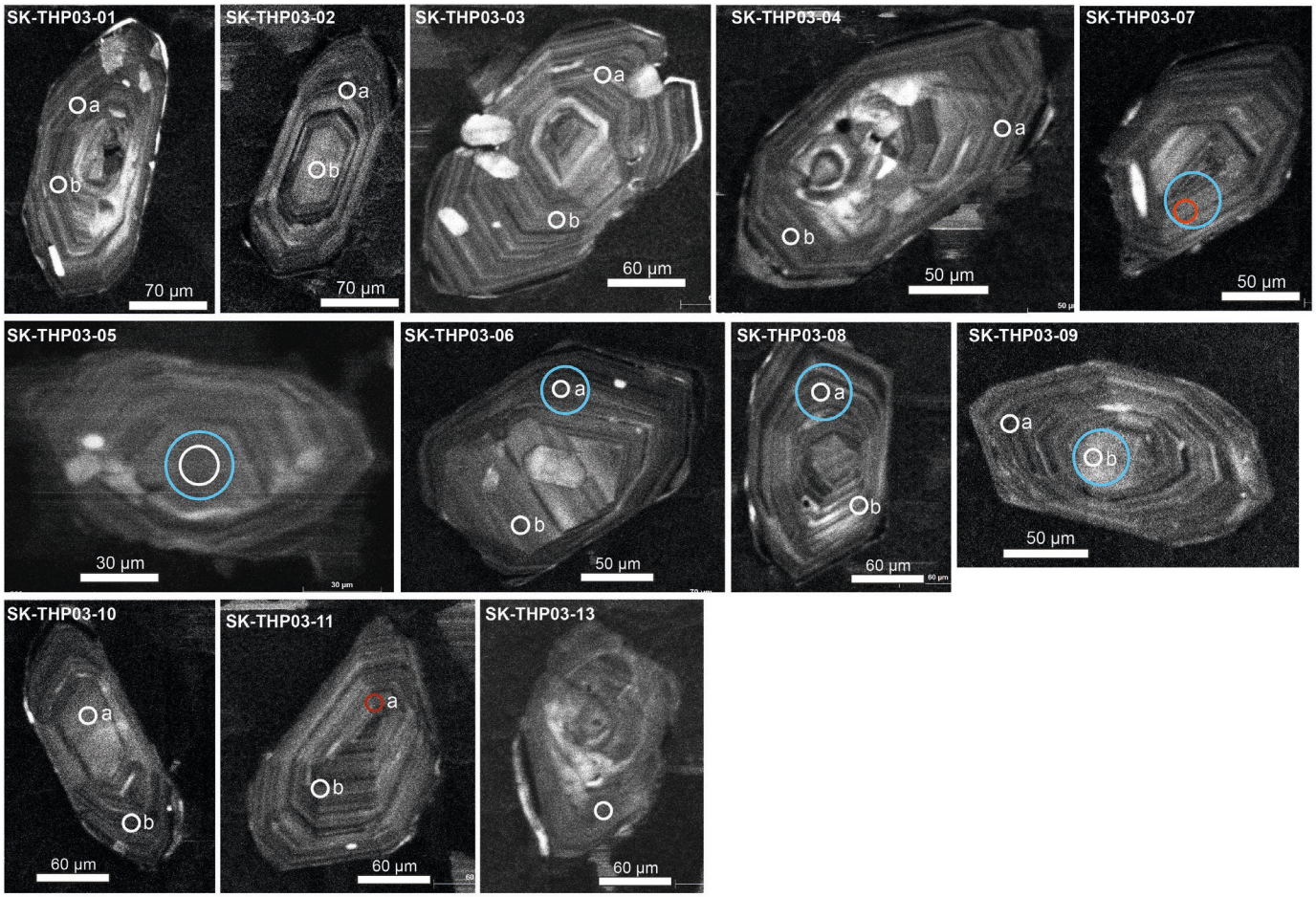

Figure S-2 Cathodoluminescence images of all analysed zircons. White circles show O isotope analysis spots (with those excluded in red), and blue circles show Si isotope analysis spots. Most analysed crystals show simple and fine oscilatory zoning, which is a typical feature of magmatic zircon crystals (e.g., Corfu *et al.*, 2003). Limited metamorphic recrystallisation and/or metasomatic alteration textures were observed, and avoided for analyses, as well as inclusions.

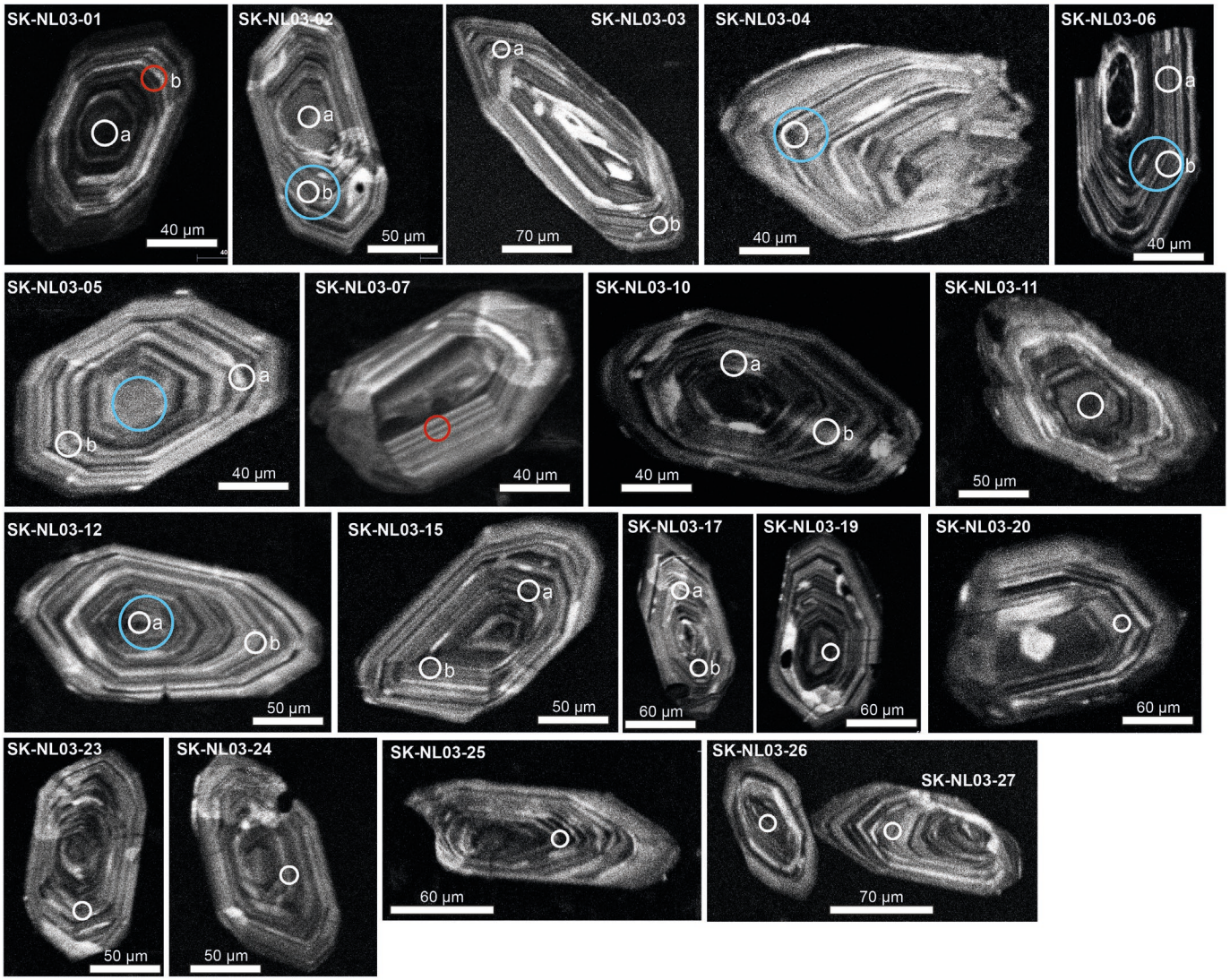

Figure S-2 (continued)

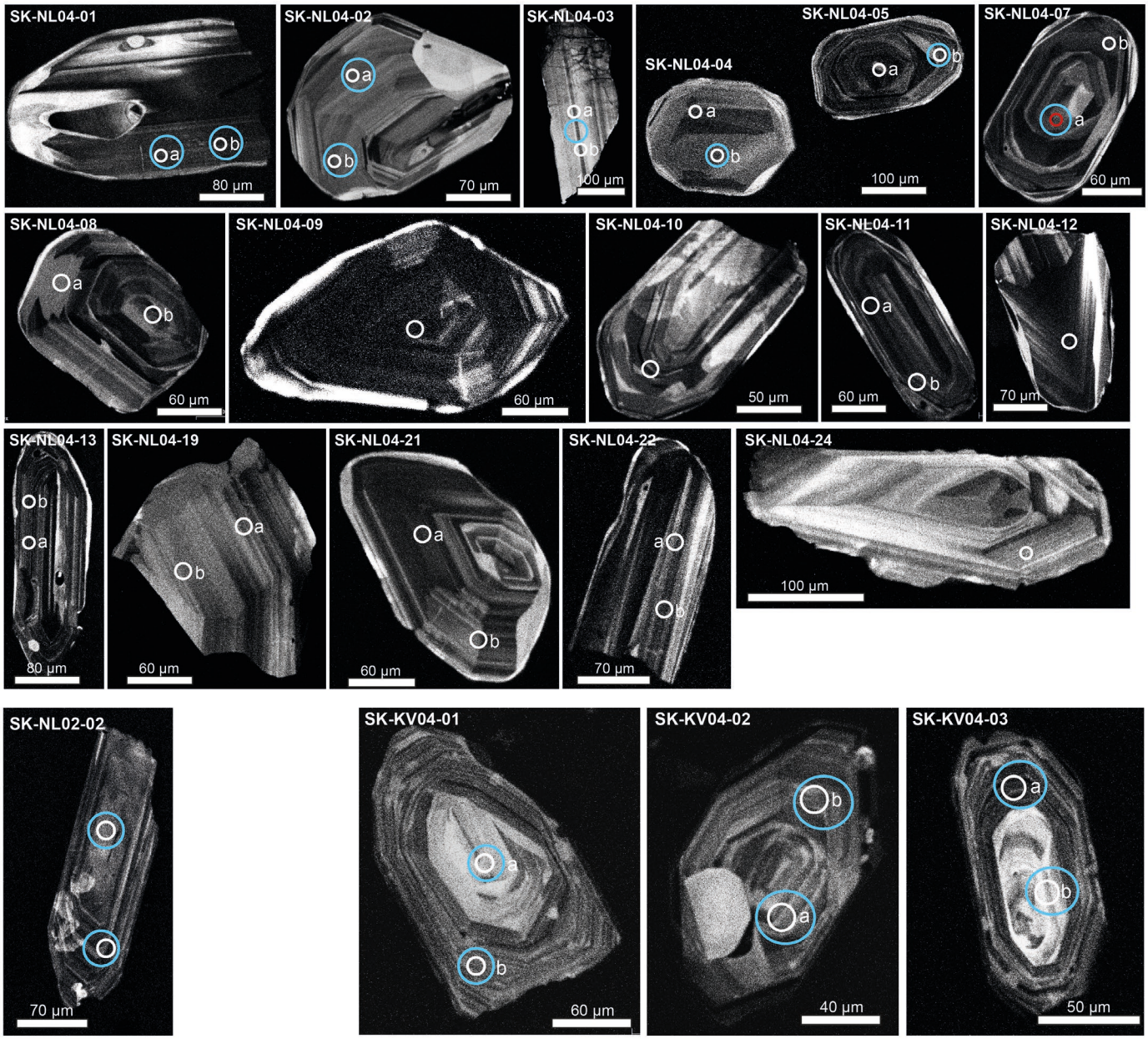

Figure S-2 (continued)

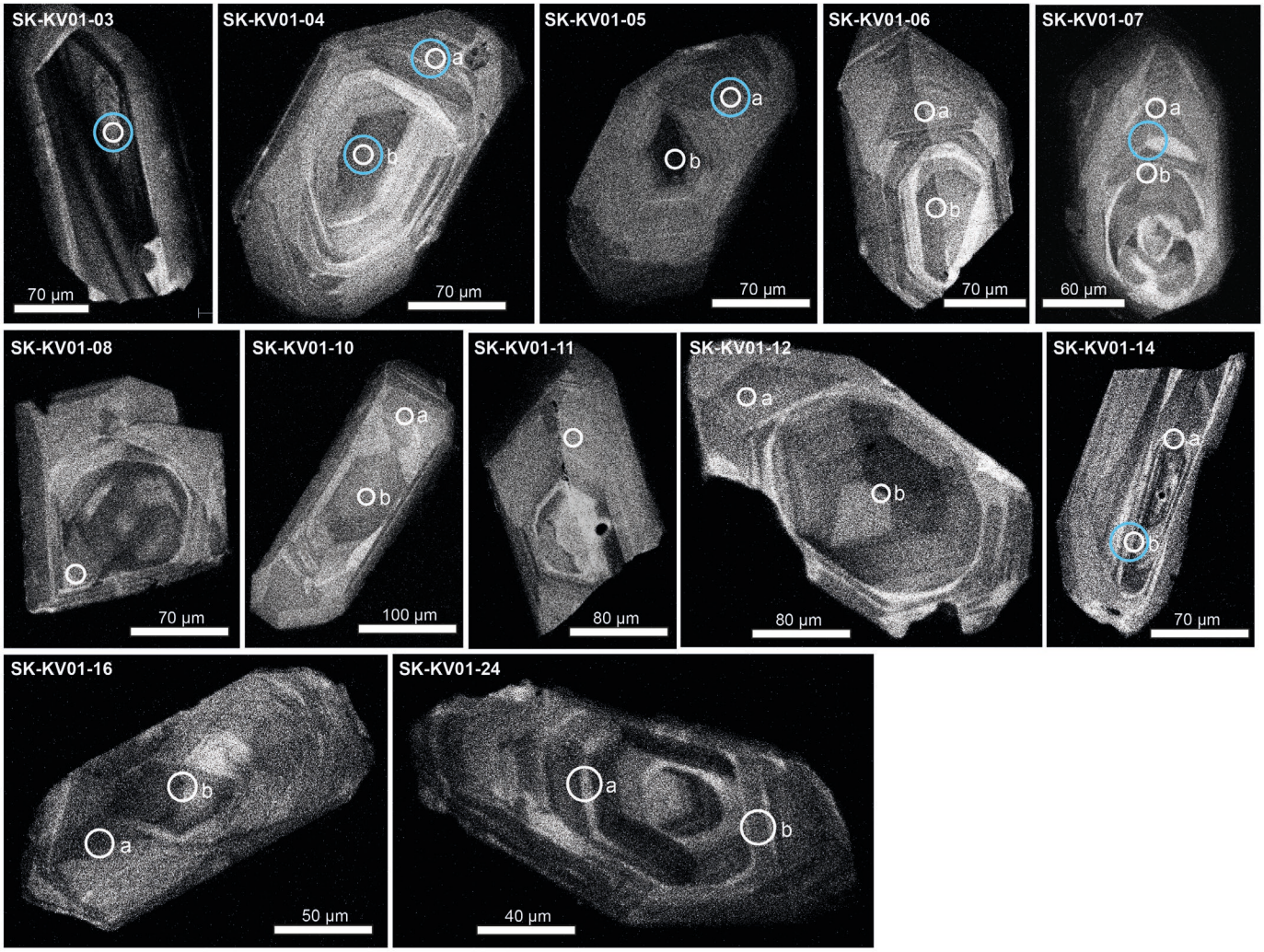

Figure S-2 (continued)

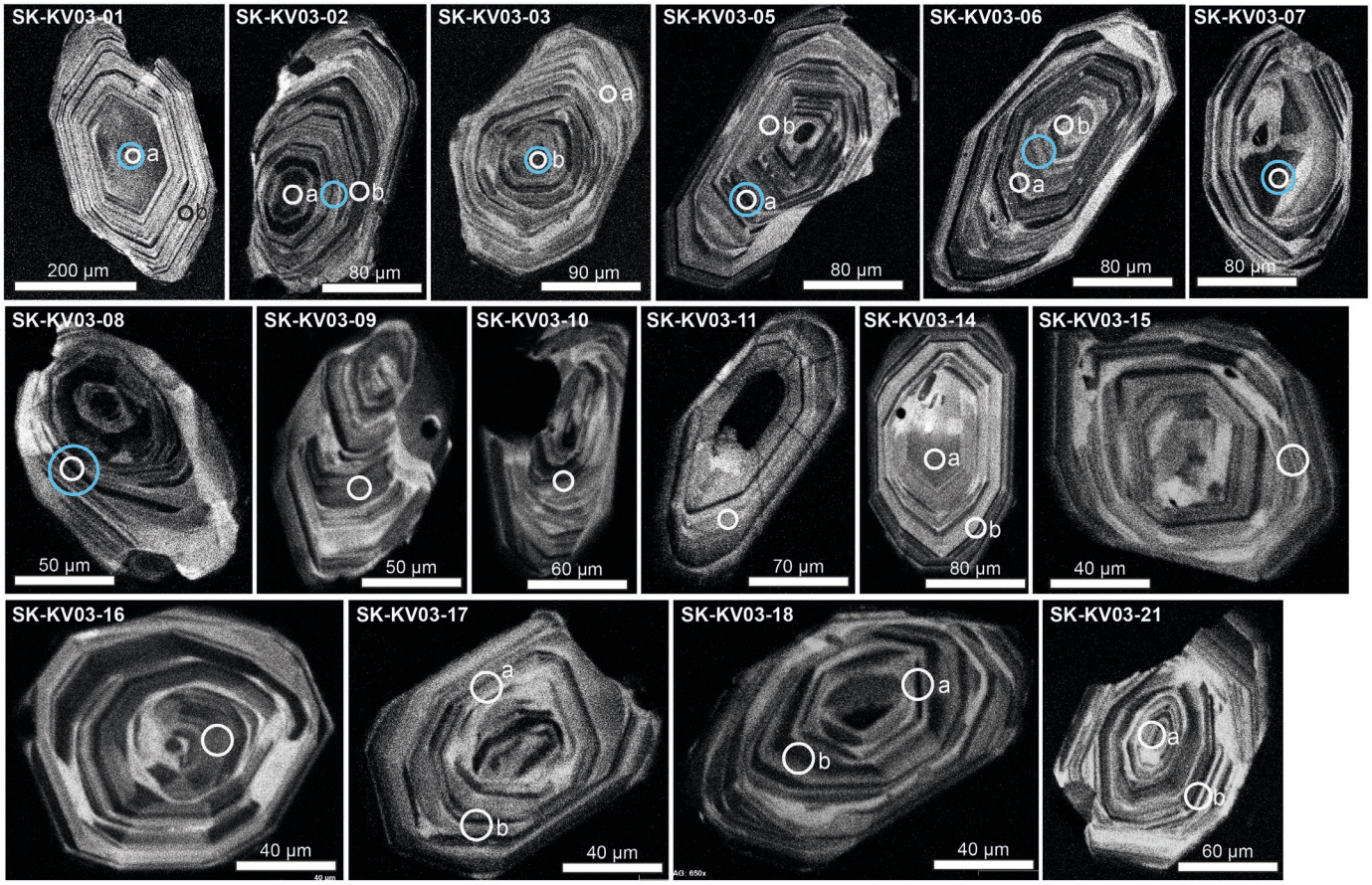

Figure S-2 (continued)

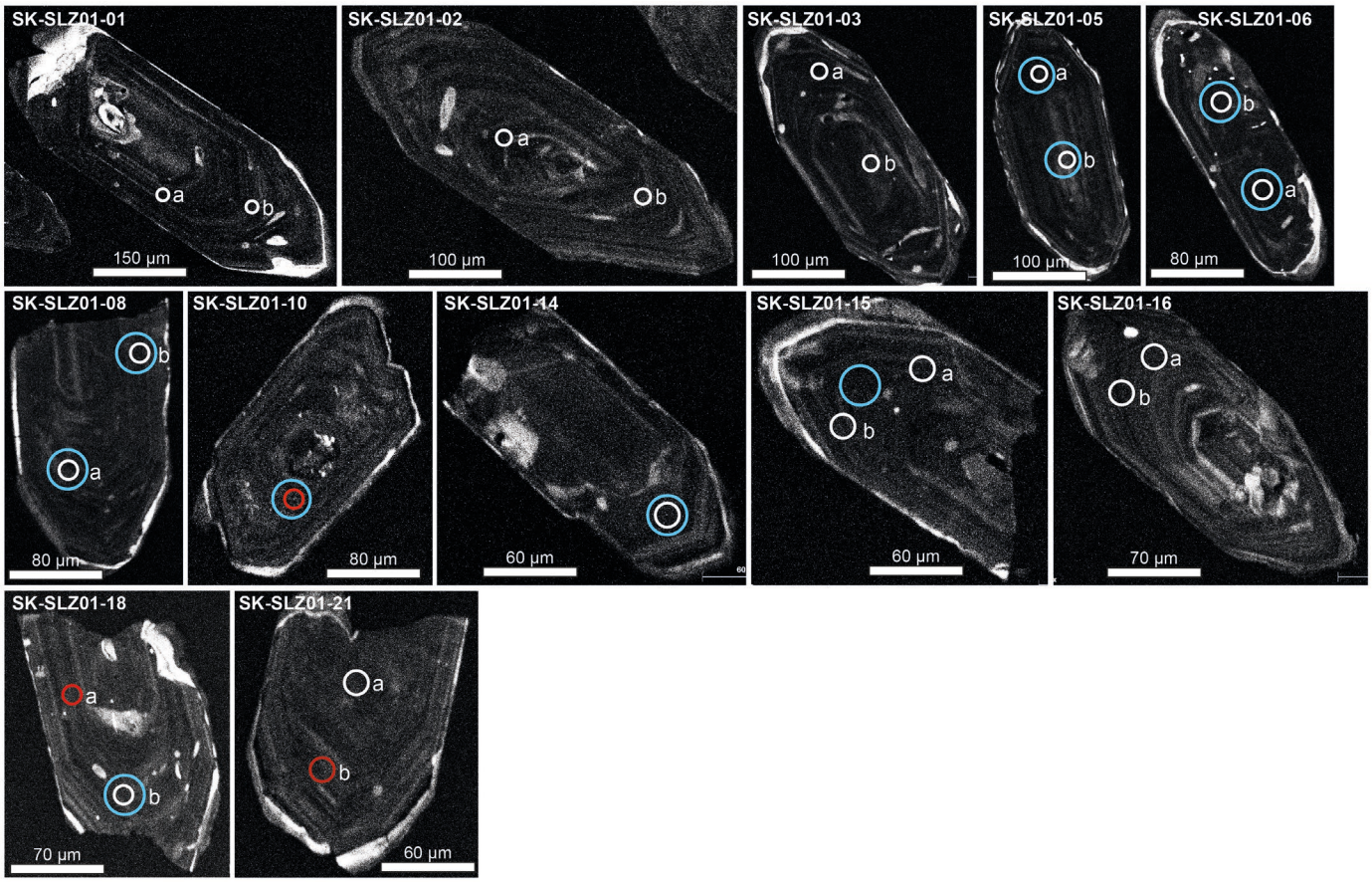

Figure S-2 (continued)

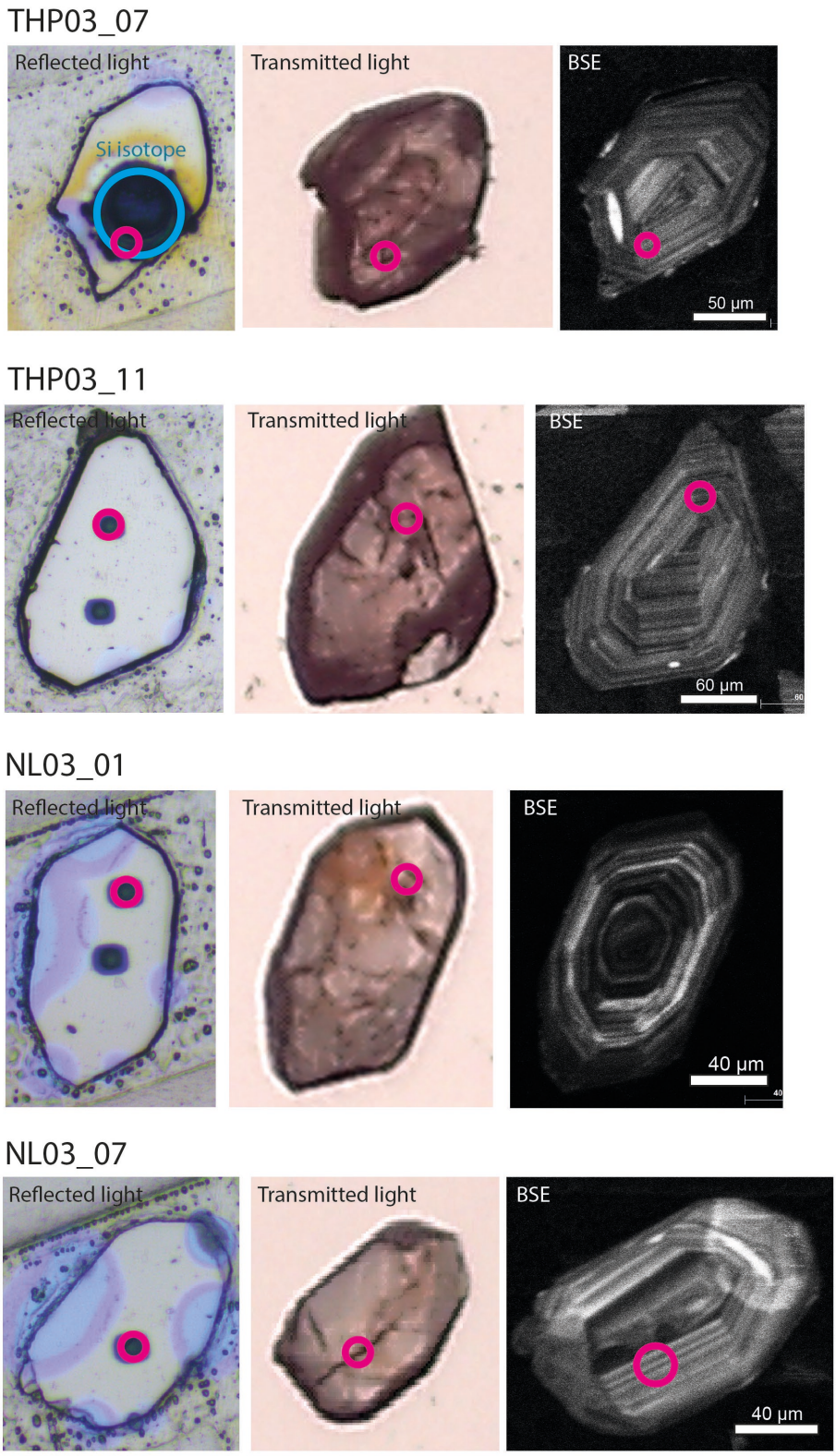

Figure S-3 Reflected and transmitted light, as well as cathodoluminescence (CL) images of zircon crystals for which some O isotope analyses were discarded (reddish pink spots) due to likely alteration and/or weathering. All of these data were acquired in seemingly simple and pristine igneous domains, as judging from CL and reflected light images, but transmitted light images revealed that these measurements were actually done on top of major cracks or tiny

fracture networks located underneath crystal surfaces. We, consequently, interpreted measured O isotope signatures as no longer primary and, instead, most likely attesting to isotope exchange that was achieved through fluid circulation through cracks and very dark (radiation-damaged) domains as already documented by several detailed studies (e.g., Pidgeon *et al*., 2017, 2019; Liebmann *et al.*, 2021; Zakharov *et al.*, 2025). The zircon crystal SLZ01-10 is quite revealing of such issues. In fact, it exhibits very dark and faint zoning with tiny bright flakes in CL, altogether pointing to important radiation damage accumulation that is a pre-requisite for effective zircon alteration (e.g., Corfu *et al.*, 2003; Pidgeon *et al.*, 2017; Guitreau *et al.*, 2018; Guitreau and Flahaut, 2019). This crystal is probably the most weathered among those discarded as argued by its CL texture but more specifically by its O and Si isotope compositions that are the lowest measured (+1.12 ‰ and -1.07 ‰, respectively). These signatures comply with those expected for low-temperature weathering, as notably noted by Pidgeon *et al.* (2017) for O isotopes and Guitreau *et al.* (2022) for Si isotopes, which partly accounts for isotope data variability in very old crystals.

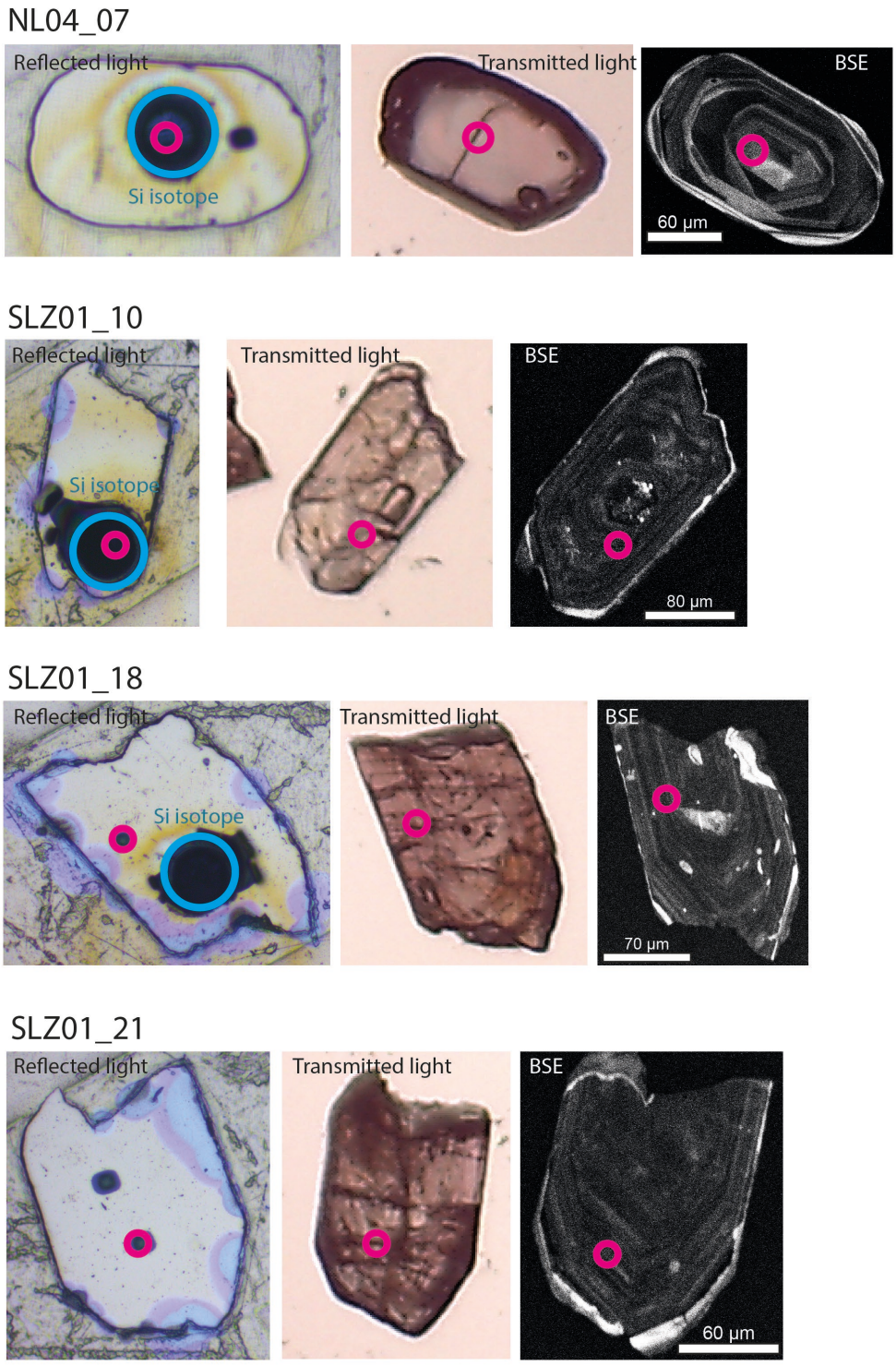

Figure S-3 (continued)

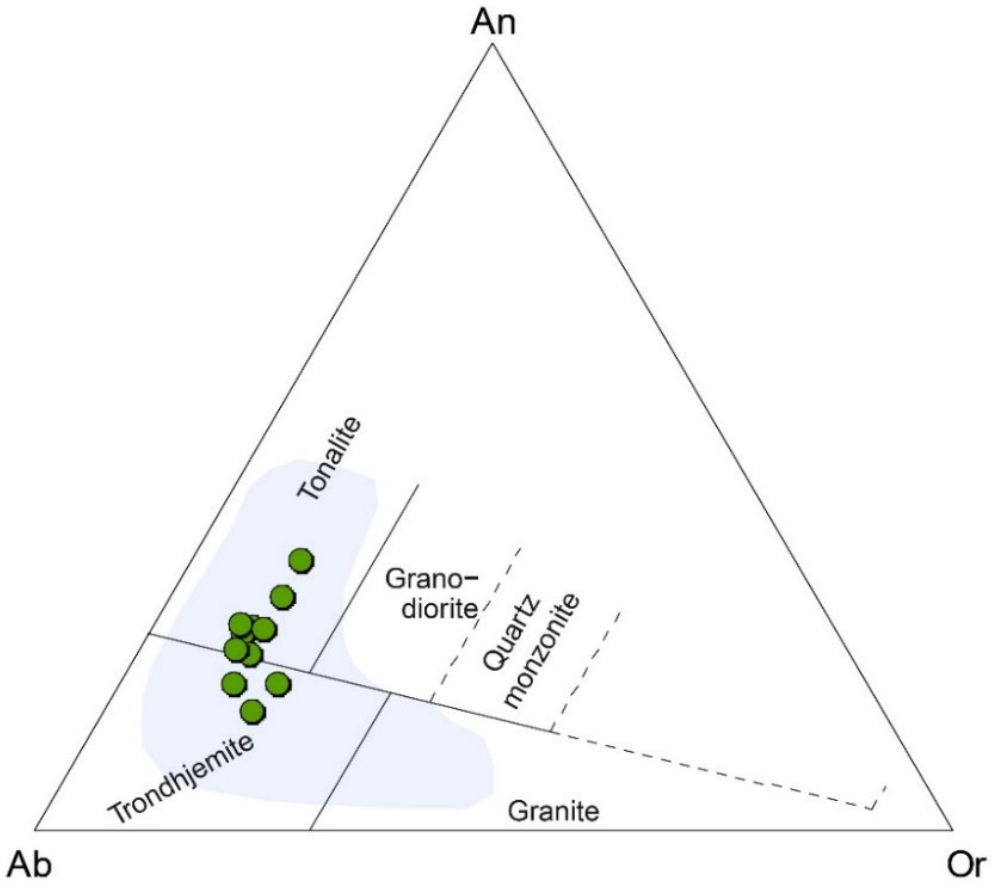

Figure S-4 Classification of the analysed Barberton TTG samples (green circles) in the An-Ab-Or diagram. The bluish field is the field of published Barberton TTG compositions (Moyen *et al.*, 2019).

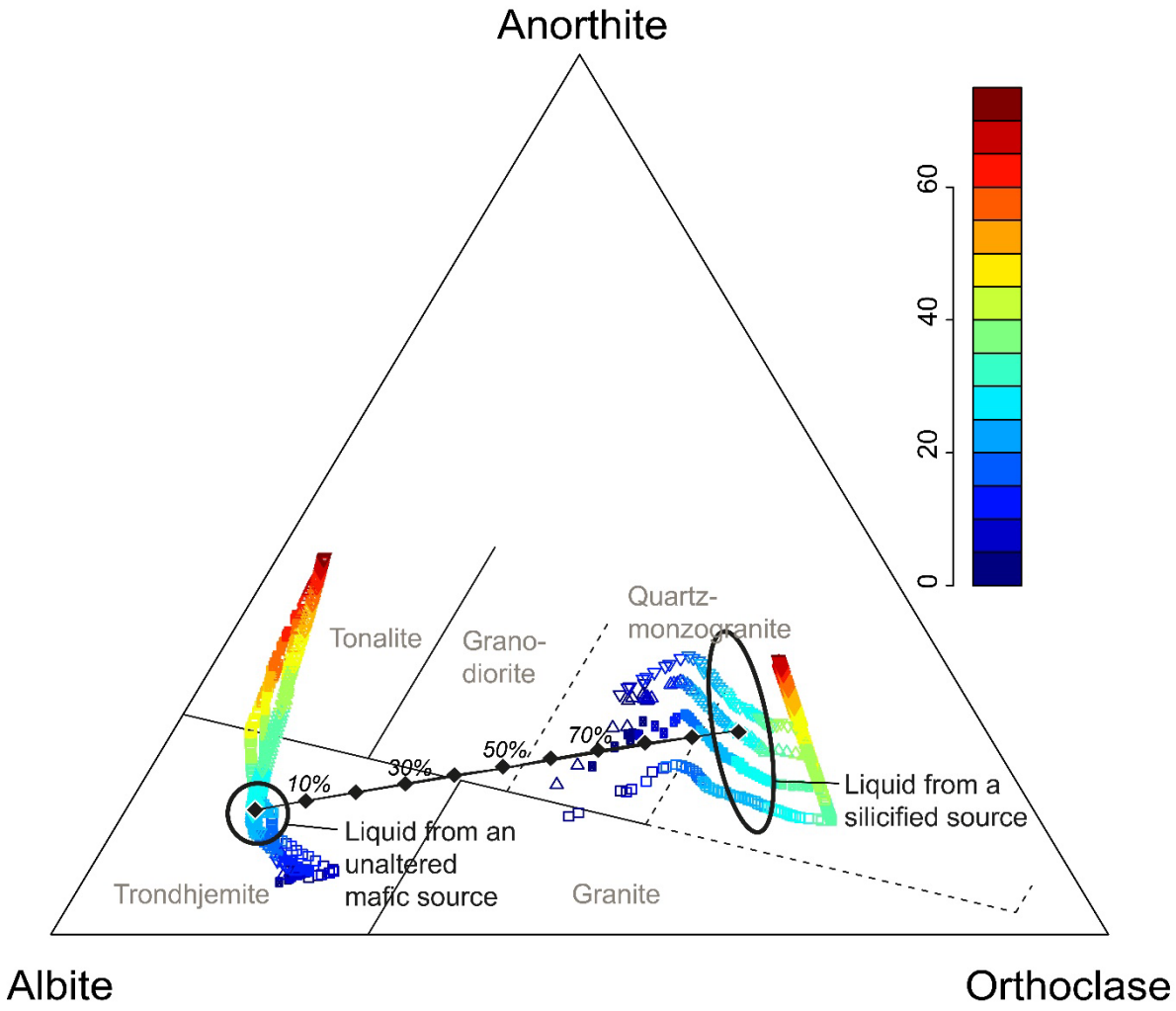

Figure S-5 Modelled liquid compositions presented in an An-Ab-Or diagram. The colour coding reflects the liquid proportion in wt. %. Black circle/ellipse represents melting conditions where a primary TTG liquid is produced. The black line shows compositions of melts obtained by mixing the liquids generated by an unaltered mafic source with those generated by a silicified seafloor source. Note the mixed liquid can contain up to 30 % of melt generated by a silicified source and still remain in the natural TTG field.

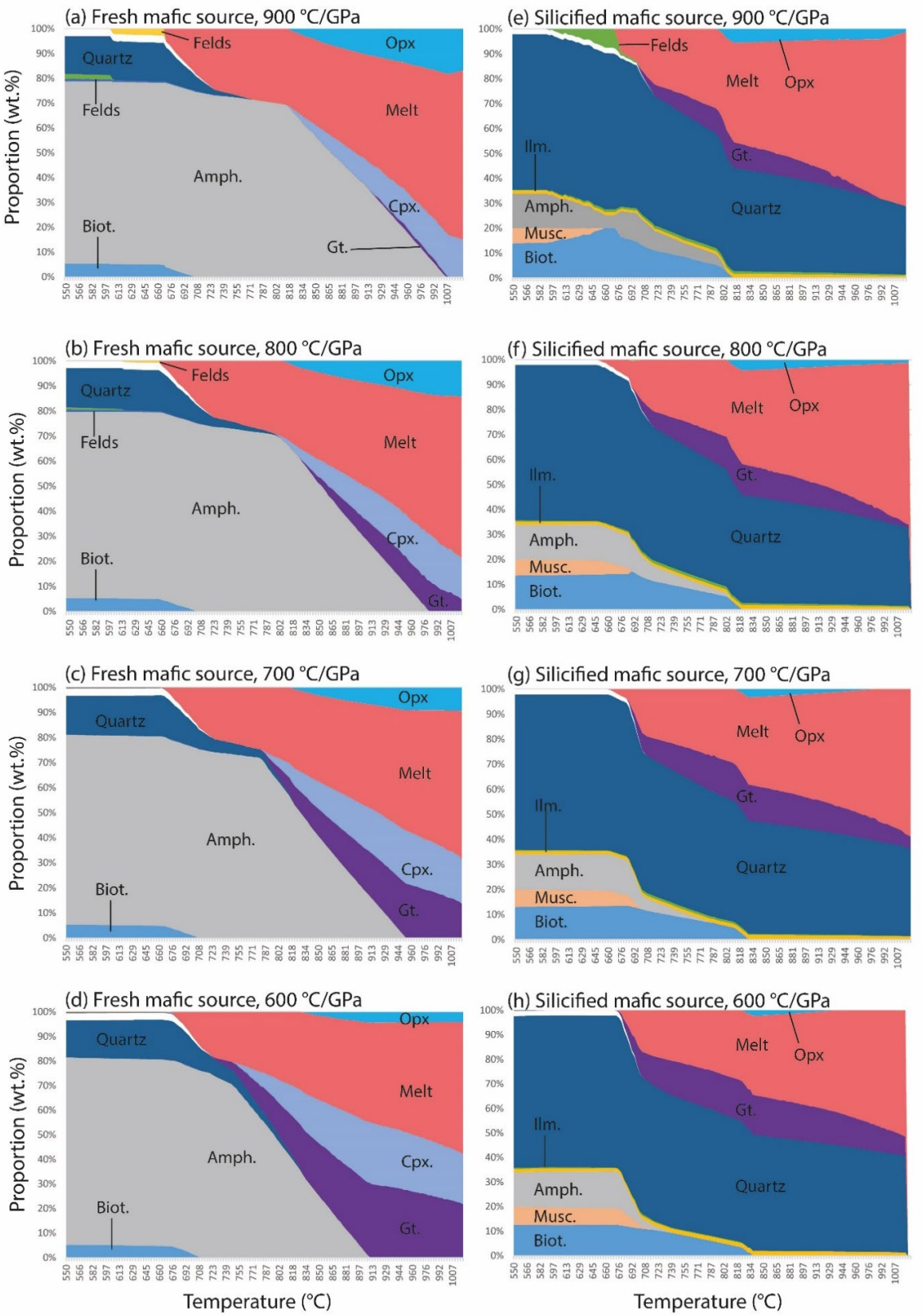

Figure S-6 Proportions of mineral phases equilibrating with the liquid at different temperatures along four different geotherms (600 °C/GPa, 700 °C/GPa, 800 °C/GPa and 900 °C/GPa). (a), (b), (c) and (d) reflect an average fresh mafic source whereas (e), (f), (g) and (h) are based on an average silicified mafic source.

Supplementary Information References

Abraham, K., Hofmann, A., Foley, S.F., Cardinal, D., Harris, C., Barth, M.G., Andre, L. (2011) Coupled silicon-oxygen isotope fractionation traces Archaean silicification. *Earth and Planetary Science Letters 301*, 222–230. https://doi.org/10.1016/j.epsl.2010.11.002

André, L., Monin, L., Hofmann, A. (2022) The origin of early continental crust: New clues from coupling Ge/Si ratios with silicon isotopes. *Earth and Planetary Science Letters 582*. https://doi.org/10.1016/j.epsl.2022.117415

Bell, E.A., Harrison, T.M. (2013) Post-Hadean transitions in Jack Hills zircon provenance : A signal of the Late Heavy Bombardment ? *Earth and Planetary Science Letters 364*, 1–11. https://doi.org/10.1016/j.epsl.2013.01.001

Bell, E.A., Harrison, T M., Mcculloch, M.T., Young, E.D. (2011) Early Archean crustal evolution of the Jack Hills Zircon source terrane inferred from Lu – Hf , 207 Pb / 206 Pb , and d 18 O systematics of Jack Hills zircons. *Geochimica et Cosmochimica Acta 75*, 4816–4829. https://doi.org/10.1016/j.gca.2011.06.007

Bindeman, I.N., Eiler, J.M., Yogodzinski, G.M., Tatsumi, Y., Stern, C.R., Grove, T.L., Portnyagin, M., Hoernle, K., Danyushevsky, L.V. (2005) Oxygen isotope evidence for slab melting in modern and ancient subduction zones. *Earth and Planetary Science Letters 235*, 480–496. https://doi.org/10.1016/j.epsl.2005.04.014

Bucholz, C.E., Jagoutz, O., Vantongeren, J.A., Setera, J., Wang, Z. (2017) Oxygen isotope trajectories of crystallizing melts : Insights from modeling and the plutonic record. *Geochimica et Cosmochimica Acta 207*, 154–184. https://doi.org/10.1016/j.gca.2017.03.027

Byerly, G.R., Lowe, D.R., Heubeck, C. (2019) Geologic Evolution of the Barberton Greenstone Belt—A Unique Record of Crustal Development, Surface Processes, and Early Life 3.55–3.20 Ga. In *Earth's Oldest Rocks*. Elsevier B.V. https://doi.org/10.1016/b978-0-444-63901-1.00024-1

Chowdhury, W., Trail, D., Guitreau, M., Bell, E., Mojzsis, S., Chowdhury, W., Trail, D., Guitreau, M., Bell, E., Buettner, J. (2021) Geochemical and textural investigations of the Eoarchean Ukaliq supracrustals , Northern Québec (Canada). *Lithos 372-373*. https://doi.org/10.1016/j.lithos.2020.105673.

Chowdhury, W., Trail, D., Miller, M., Savage, P. (2023) Eoarchean and Hadean melts reveal arc-like trace element and isotopic signatures. *Nature Communications 14*. https://doi.org/10.1038/s41467-023-36538-5

Corfu, F., Hanchar, J. M., Hoskin, P. W. O., Kinny, P. (2003. Atlas of zircon textures. *Reviews in Mineralogy and Geochemistry* 53, 469–500.

de Wit, M.J., Furnes, H. (2016) 3.5-Ga hydrothermal fields and diamictites in the Barberton Greenstone Belt-Paleoarchean crust in cold environments. *Science Advances 2*, 1–12. https://doi.org/10.1126/sciadv.1500368

Faure, K., Harris, C. (1991) Oxygen and carbon isotope geochemistry of the 3 . 2 Ga Kaap Valley tonalite , Barberton greenstone belt , South Africa. *Precambrian Research 52*, 301–319.

Fourie, D.S., Harris, C. (2011) O-isotope study of the bushveld complex granites and granophyres: Constraints on source composition, and assimilation. *Journal of Petrology 52*, 2221–2242. https://doi.org/10.1093/petrology/egr045

Furnes, H., Robins, B., De Wit, M.J. (2012) Geochemistry and petrology of lavas in the upper onverwacht suite, Barberton Mountain Land, South Africa. *South African Journal of Geology 115*, 171–210. https://doi.org/10.2113/gssajg.115.2.171

Guitreau, M., Gannoun, A., Deng, Z., Chaussidon, M., Moynier, F., Barbarin, B., Marin-Carbonne, J. (2022) Stable isotope geochemistry of silicon in granitoid zircon. *Geochimica et Cosmochimica Acta 316*, 273–294. https://doi.org/10.1016/j.gca.2021.09.029

Guitreau, M., Gannoun, A., Deng, Z., Marin-Carbonne, J., Chaussidon, M., Moynier, F. (2020) Silicon isotope measurement in zircon by laser ablation multiple collector inductively coupled plasma mass spectrometry. *Journal of Analytical Atomic Spectrometry 35*, 1597–1606. https://doi.org/10.1039/d0ja00214c

Guitreau, M., Flahaut, J. (2019) Record of low-temperature aqueous alteration of Martian zircon during the late Amazonian. *Nature Communications* 10, 2457. doi: 10.1038/s41467-019-10382-y

Guitreau, M., Mora, N., Paquette, J. (2018) Crystallization and disturbance histories of single zircon crystals from Hadean–Eoarchean Acasta gneisses examined by LA-ICP-MS U–Pb traverses. *Geochemistry, Geophysics, Geosystems* 19, 272–291, https://doi.org/10.1002/2017GC007310

Hiess, J., Bennett, V.C., Nutman, A.P., Williams, I.S. (2011) *Archaean fluid-assisted crustal cannibalism recorded by low d 18 O and negative e Hf (T) isotopic signatures of West Greenland granite zircon*. 1027–1050. https://doi.org/10.1007/s00410-010-0578-z

Hofmann, A., Harris, C. (2008) Silica alteration zones in the Barberton greenstone belt : A window into subseafloor processes 3.5-3.3 Ga ago. *Chemical Geology 257*, 224–242. https://doi.org/10.1016/j.chemgeo.2008.09.015

Holland, T.J.B., Green, E.C.R., Powell, R. (2018) Melting of peridotites through to granites: A simple thermodynamic model in the system KNCFMASHTOCr. *Journal of Petrology 59*, 881–900. https://doi.org/10.1093/petrology/egy048

Holland, T.J.B., Powell, R. (2011) An improved and extended internally consistent thermodynamic dataset for phases of petrological interest, involving a new equation of state for solids. *Journal of Metamorphic Geology 29*, 333–383. https://doi.org/10.1111/j.1525-1314.2010.00923.x

Kitoga, L.S., Zakharov, D., Marin-Carbonne, J., Boyet, M., Moyen, J.-F., Di Rocco, T., Pack, A., Olivier, N., Stevens, G. (2024) Oxygen and silicon isotopic compositions of Archean silicified lava and cherts of the Onverwacht Group: Implication for seafloor hydrothermalism and the nature of recycled components in the source of granitoids. *Chemical Geology* 122407. https://doi.org/10.1016/j.chemgeo.2024.122407

Lackey, J.S., Valley, J.W., Chen, J.H., Stockli, D.F. (2008) Dynamic magma systems, crustal recycling, and alteration in the Central Sierra Nevada batholith: The oxygen isotope record. *Journal of Petrology 49*, 1397–1426. https://doi.org/10.1093/petrology/egn030

Lahaye, Y., Arndt, N., Byerly, G., Chauvel, C., Fourcade, S., Gruau, G. (1995) The influence of alteration on the trace-element and Nd isotopic compositions of komatiites. *Chemical Geology 126*, 43–64.

Lei, K., Wang, H., Wang, X., Zhang, Q., Li, X. (2023) Decoupled Zircon Si–O Isotopes Tracing the Supracrustal Silicification and Komatiitic-Derived Fluids in the Source of TTGs. *Geophysical Research Letters 50*, 1–9. https://doi.org/10.1029/2023GL104002

Liebmann, J., Spencer, C.J., Kirkland, C.L., Xia, X.-P., Bourdet, J. (2021) Effect of water on **δ**18O in zircon. *Chemical Geology* 574, 120243, https://doi.org/10.1016/j.chemgeo.2021.120243

Lowe, D.R., Byerly, G.R. (2007) An overview of the geology of the Barberton greenstone belt and vicinity: implications for early crustal development. In M.J. Van Kranendonk, R H. Smithies, V.C. Bennett (Eds.), *Developments in Precambrian Geology* (Vol. 15, Issue 07, pp. 481–526). Elsevier B.V. https://doi.org/10.1016/S0166-2635(07)15053-2

Mayne, M.J., Stevens, G., Moyen, J.-F. (2019) *A phase equilibrium investigation of selected source controls on the composition of melt batches generated by sequential melting of an average metapelite*. https://doi.org/10.6084/m9.figshare.c.4601786

Moyen, J.-F., Stevens, G., Kisters, A.F.M., Belcher, R.W., Lemirre, B. (2019) TTG Plutons of the Barberton Granitoid-Greenstone

Terrain, South Africa. In *Earth's Oldest Rocks*. https://doi.org/10.1016/b978-0-444-63901-1.00025-3

Moyen, J.F., Zeh, A., Cuney, M., Dziggel, A., Carrouée, S. (2021) The multiple ways of recycling Archaean crust: A case study from the ca. 3.1 Ga granitoids from the Barberton Greenstone Belt, South Africa. *Precambrian Research*, *353*(November 2020), 105998. https://doi.org/10.1016/j.precamres.2020.105998

Murphy, M.E., Macdonald, J.E., Fischer, S., Gardiner, N.J., White, R.W., Savage, P.S. (2024) Silicon isotopes in an Archaean migmatite confirm seawater silicification of TTG sources. *Geochimica et Cosmochimica Acta 368*, 34–49. https://doi.org/10.1016/j.gca.2024.01.018

Pack, A., Herwartz, D. (2014) The triple oxygen isotope composition of the Earth mantle and understanding δO17 variations in terrestrial rocks and minerals. *Earth and Planetary Science Letters 390*, 138–145. https://doi.org/10.1016/j.epsl.2014.01.017

Pack, A., Tanaka, R., Hering, M., Sengupta, S., Peters, S., Nakamura, E. (2016) The oxygen isotope composition of San Carlos olivine on the VSMOW2-SLAP2 scale. *Rapid Communications in Mass Spectrometry*, *April*, 1495–1504. https://doi.org/10.1002/rcm.7582

Pidgeon R.T., Nemchin A.A., Whitehouse M.J. (2017) The effect of weathering on U-Th-Pb and oxygen isotope system of ancient zircons from the Jack Hills, Western Australia. *Geochimica et Cosmochimica Acta* 197, 142–166.

Pidgeon, R.T., Nemchin, A., Roberts, M., Whitehouse, M.J., Bellucci, J. (2019) The accumulation of nonformula elements in zircons during weathering: ancient zircons from the Jack Hills, Western Australia. *Chemical Geology* 530, 19310, https://doi.org/10.1016/j.chemgeo.2019.119310

Puchtel, I.S., Blichert-Toft, J., Touboul, M., Walker, R.J., Byerly, G.R., Nisbet, E.G., Anhaeusser, C.R. (2013) Insights into early Earth from Barberton komatiites: Evidence from lithophile isotope and trace element systematics. *Geochimica et Cosmochimica Acta*, *108*, 63–90. https://doi.org/10.1016/j.gca.2013.01.016

Roberts, N.M.W., Santosh, M. (2018) Capturing the Mesoarchean Emergence of Continental Crust in the Coorg Block, Southern India. *Geophysical Research Letters 45*, 7444–7453. https://doi.org/10.1029/2018GL078114

Savage, P.S., Georg, R.B., Armytage, R.M.G., Williams, H.M., Halliday, A.N. (2010) Silicon isotope homogeneity in the mantle. *Earth and Planetary Science Letters 295*, 139–146. https://doi.org/10.1016/j.epsl.2010.03.035

Schneider, K.P., Hoffmann, J.E., Münker, C., Patyniak, M., Sprung, P., Roerdink, D., Wissenschaften, G., Berlin, F.U. (2019) Petrogenetic evolution of metabasalts and metakomatiites of the lower Onverwacht Group , Barberton Greenstone Belt (South Africa). *Chemical Geology 511*, 152–177. https://doi.org/10.1016/j.chemgeo.2019.02.020

Shieh, Y.-N., Schwarcz, H.P. (1974) *Oxygen isotope studies of granite and migmatite, Grenville province of Ontario, 38*.

Smithies, R.H., Lu, Y., Kirkland, C.L., Johnson, T.E., Mole, D.R., Champion, D.C., Martin, L., Jeon, H., Wingate, M.T.D., Johnson, S.P. (2021) Oxygen isotopes trace the origins of Earth ' s earliest continental crust. *Nature 592*. https://doi.org/10.1038/s41586-021-03337-1

Trail, D., Boehnke, P., Savage, P.S., Liu, M.C., Miller, M.L., Bindeman, I. (2018). Origin and significance of Si and O isotope heterogeneities in Phanerozoic, Archean, and Hadean zircon. *Proceedings of the National Academy of Sciences of the United States of America 115*, 10287–10292. https://doi.org/10.1073/pnas.1808335115

Valley, J.W., Chiarenzelli, J.R., McLelland, J.M. (1994) Oxygen isotope geochemistry of zircon. *Earth and Planetary Science Letters*, *126*(4), 187–206. https://doi.org/10.1016/0012-821X(94)90106-6

Valley, J.W., Lackey, J.S., Cavosie, A.J., Clechenko, C.C., Spicuzza, M.J., Basei, M.A.S., Bindeman, I.N., Ferreira, V.P., Sial, A. N., King, E.M., Peck, W.H., Sinha, A.K., Wei, C.S. (2005) 4.4 billion years of crustal maturation: Oxygen isotope ratios of

magmatic zircon. *Contributions to Mineralogy and Petrology 150*, 561–580. https://doi.org/10.1007/s00410-005-0025-8

Vezinet, A., Pearson, D.G., Thomassot, E., Stern, R.A., Sarkar, C., Luo, Y., Fisher, C.M. (2018) Hydrothermally-altered mafic crust as source for early Earth TTG: Pb/Hf/O isotope and trace element evidence in zircon from TTG of the Eoarchean Saglek Block, N. Labrador. *Earth and Planetary Science Letters*, *503*, 95–107. https://doi.org/10.1016/j.epsl.2018.09.015

Vezinet, A., Thomassot, E., Pearson, D.G., Stern, R.A., Luo, Y., Sarkar, C. (2019) Extreme δ18O signatures in zircon from the Saglek Block (North Atlantic Craton) document reworking of mature supracrustal rocks as early as 3.5 Ga. *Geology*, *47*, 605–608. https://doi.org/10.1130/G46086.1

Wang, X., Tang, M., Moyen, J., Wang, D., Kröner, A., Xia, X., Xie, H., Anhaeusser, C., Hofmann, A., Li, J., Li, L. (2022) The onset of deep recycling of supracrustal materials at the Paleo-Mesoarchean boundary. *National Science Review*, *9*, 1–9.

Wiedenbeck, M., Hanchar, J.M., Peck, W.H., Sylvester, P., Valley, J., Whitehouse, M., Kronz, A., Morishita, Y., Nasdala, L. (2004) Further Characterisation of the 91500 Zircon Crystal. *Geostandards and Geoanalytical Research*, *28*, 9–39. https://doi.org/10.1111/j.1751-908X.2004.tb01041.x

Zakharov, D., Paul, A.N. Colòn, D.P., Ovtcharova, M., Putlitz, B., Bouvier, A.-S., Sheik, A.A., Zozulya, D., Robyr, M. (2025) Low-δ18O (-8 ‰, VSMOW) Paleoproterozoic and discordant zircon: Lessons learned from using a combination of traditional bulk and in situ approaches. *Chemical Geology* 693, 122972. https://doi.org/10.1016/j.chemgeo.2025.122972

Zeh, A., Stern, R.A., Gerdes, A. (2014) The oldest zircons of Africa — Their U – Pb – Hf – O isotope and trace element systematics , and implications for Hadean to Archean crust – mantle evolution. *Precambrian Research 241*, 203–230. https://doi.org/10.1016/j.precamres.2013.11.006